AIP | The Journal of Chemical Physics

Effect of amphiphilic block copolymers on the structure and phase behavior of oil–water-surfactant mixtures

H. Endo, M. Mihailescu, M. Monkenbusch, J. Allgaier, G. Gompper, D. Richter, B. Jakobs, T. Sottmann, R. Strey , and I. Grillo

Citation: The Journal of Chemical Physics **115**, 580 (2001); doi: 10.1063/1.1377881
View online: http://dx.doi.org/10.1063/1.1377881
View Table of Contents: http://scitation.aip.org/content/aip/journal/jcp/115/1?ver=pdfcov
Published by the AIP Publishing

Articles you may be interested in

Pressure-induced hexagonal phase in a ternary microemulsion system composed of a nonionic surfactant, water, and oil
J. Chem. Phys. **123**, 054705 (2005); 10.1063/1.1993559

Dynamic properties of microemulsions modified with homopolymers and diblock copolymers: The determination of bending moduli and renormalization effects
J. Chem. Phys. **122**, 094908 (2005); 10.1063/1.1857523

Oil-in-water microemulsions stabilized by charged diblock copolymers
J. Chem. Phys. **122**, 064703 (2005); 10.1063/1.1845396

Structural transformations in confined lamellar phases in oil–water–surfactant mixtures
J. Chem. Phys. **115**, 8705 (2001); 10.1063/1.1412606

Small-angle scattering of interacting particles. III. D 2 O-C 12 E 5 mixtures and microemulsions with n -octane
J. Chem. Phys. **110**, 10623 (1999); 10.1063/1.478993

Reuse of AIP Publishing content is subject to the terms: https://publishing.aip.org/authors/rights-and-permissions. Downloaded to IP: 145.94.180.253 On: Thu, 17 Mar 2016 15:06:52

Effect of amphiphilic block copolymers on the structure and phase behavior of oil–water-surfactant mixtures

H. Endo, M. Mihailescu, M. Monkenbusch, J. Allgaier, G. Gompper, and D. Richter
Institut für Festkörperforschung, Forschungszentrum Jülich, D-52425 Jülich, Germany

B. Jakobs, T. Sottmann, and R. Strey
Institut für Physikalische Chemie, Universität zu Köln, Luxemburger Str. 116, D-50939 Köln, Germany

I. Grillo
Institut Laue Langevin, 6, rue Jules Horowitz, BP156, 38042 Grenoble Cedex 9, France

(Received 29 December 2000; accepted 16 April 2001)

The effect of amphiphilic diblock copolymers of several molecular weights on the structure and phase behavior of ternary amphiphilic systems (water, oil, and nonionic surfactant) is investigated. Small amounts of amphiphilic block copolymer polyethyleneoxide–polyethylpropylene lead to a dramatic decrease of the amount of total surfactant needed to solubilize given equal volumes of water and oil in a bicontinuous microemulsion. Neutron scattering experiments employing a high-precision two-dimensional contrast variation technique demonstrate that the polymer is distributed uniformly on the surfactant membrane. Based on these observations, we propose a mechanism for the enhancement of swelling behavior, which is due to the variation of the membrane curvature elasticity by polymer mushrooms anchored to the interface. © *2001 American Institute of Physics.* [DOI: 10.1063/1.1377881]

I. INTRODUCTION

Microemulsions are thermodynamically stable and macroscopically homogeneous mixtures of water and oil, where the miscibility is mediated by surfactant molecules. Microscopically the surfactants form an extended interfacial film separating water and oil on a local scale. Recently we discovered an enormous efficiency increase of the emulsification capacity of the nonionic surfactant $C_{10}E_4$ by adding amphiphilic block copolymers of polyethylenepropylene/polyethyleneoxide (PEP–PEO). While mixtures of two surfactants of similar chain length show only small synergistic effects in microemulsions, adding the amphiphilic block copolymer to a conventional microemulsion system was found to lead to a very large efficiency increase already for traces of polymer.[1]

The extraordinary role of polymers is not only restricted to synthetic systems like conventional microemulsions but has received also much attention in connection with amphiphilic bilayers and biological membranes. Polymers anchored to phospholipid bilayers have for example been used to protect artificial vesicles against the immune system response and make effective drug carrier systems.[2–6] Water soluble polymers anchored to lipid bilayers have also been found to exhibit a lamellar hydrogel phase at high water concentration.[7,8] When the bending rigidity of the bilayer is reduced to values of the order of the thermal energy k_BT by the addition of a cosurfactant—determined from the analysis of the scattering intensity—gelation is found to occur already in mixtures containing as little as 0.5 wt % PEO lipid.

Theoretically, the polymer decoration of membranes is expected to increase the bending rigidity. Such an effect has qualitatively been observed in the lamellar phase of membranes, to which hydrophilic polymers are anchored by hydrophobic side chains, below the overlap concentration of the polymers on the membrane.[9] Similarly, micropipet aspiration experiments[10] of vesicles with PEO lipids show an increase of the bending rigidity *above* the overlap concentration, while no data are available in this system below overlap. In both cases the bending rigidity was found to level off at higher polymer concentrations. On the other hand, the bending rigidity was found to vary little with polymer concentration both in the lamellar phases of Refs. 7 and 8 and in surfactant bilayer vesicles with PEO surfactants.[11]

Structural properties of such complex fluids may be accessed by small angle neutron scattering (SANS) which takes advantage of the unique possibility to vary the contrast between the different components by hydrogen–deuterium exchange. A number of systematic studies on bicontinuous microemulsions under either oil–water or film contrast are reported in the literature.[12–16]

The theoretical understanding of microemulsion phases has been promoted by a detailed analysis—based on statistical physics—of several classes of models of amphiphilic systems. We want to mention microscopic lattice models, Ginzburg–Landau-type free-energy functional approaches, as well as interfacial models which employ the curvature elasticity of the amphiphile film. A recent overview by Gompper and Schick[17] reviews the state of the art. In particular the Ginzburg–Landau-type theories reveal the structure factor for oil–water microemulsions under bulk-contrast conditions—the so called Teubner–Strey formula[12]—which is employed routinely in order to describe such scattering results. On the other hand, already the scattering under film contrast is much less understood. Recently, Roux *et al.*[18,19]

 © 2001 American Institute of Physics

Reuse of AIP Publishing content is subject to the terms: https://publishing.aip.org/authors/rights-and-permissions. Downloaded to IP: 145.94.180.253 On: Thu, 17 Mar 2016 15:06:52

as well as Gompper and Schick[20] presented Ginzburg–Landau models with two scalar order parameters, in order to describe the thermal fluctuations of the amphiphile density in microemulsions, which was shown to be strongly influenced by the oil–water correlation function. Alternatively, Pieruschka and Safran[21,22] have calculated the scattering intensities under bulk and film contrast within the interfacial approach.

Finally, the phase diagrams of microemulsions are strongly influenced by the elastic moduli, the bending modulus κ and the saddle splay or Gaussian curvature modulus $\bar{\kappa}$, of the surfactant film. Recently, Morse,[23] Golubovic,[24] and Gompper and Kroll[25] demonstrated an exponential dependence of the phase boundary of the homogeneous phase in terms of the surfactant volume fraction on the magnitude of the saddle-splay modulus $\bar{\kappa}$. Polymers tethered to a surfactant layer modify the elasticity moduli and thus are expected to have a profound effect on the phase diagrams.

In this paper we display a coherent set of scattering results on bicontinuous microemulsions with varying polymer concentration. We evaluate the different partial structure factors and interpret the results for the bulk and film contrasts jointly in terms of both Ginzburg–Landau and interfacial models. We study the effect of the polymers on the various parameters of the theory and evaluate the system parameters on the basis of the structural information. Furthermore, the polymer scattering by itself is studied in extracting the polymer–polymer partial structure factor. This quantity provides information about the polymer conformation and polymer density in the system. In particular, we show that all polymer chains are tethered to the surfactant films. A schematic illustration of the microemulsion structure containing block copolymer is given by Fig. 1. Detailed information on the density profile of the tethered chains are also obtained from the interference term between the polymer and the film scattering. Finally, the efficiency boosting effect of the tethered polymers is explained in terms of the variation of the saddle-splay modulus $\bar{\kappa}$ by the tethered chains.[26]

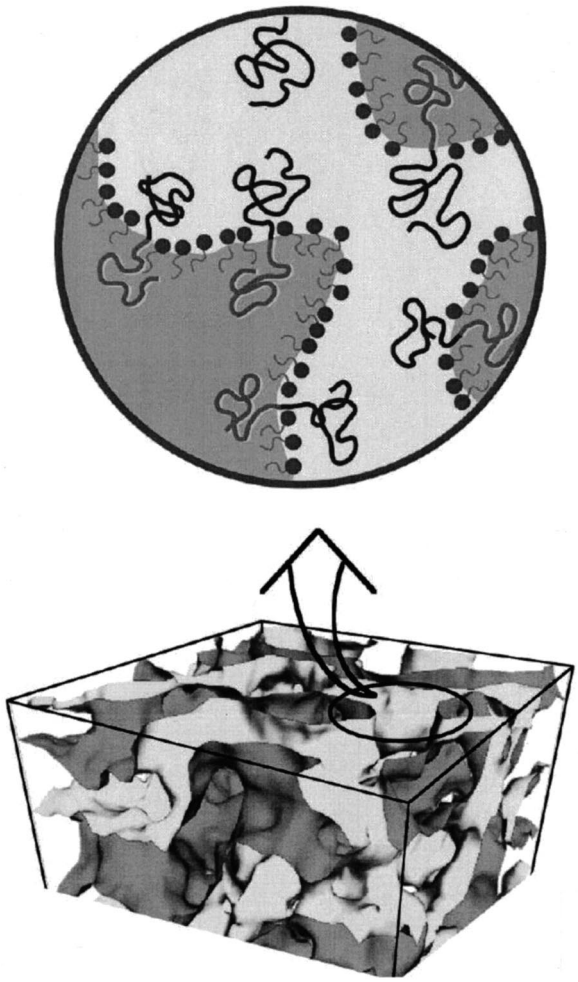

FIG. 1. Schematic illustration of the bicontinuous microemulsion structure and the polymer distribution on the interface as inferred from the experimental results presented in this paper.

II. EXPERIMENTAL SECTION

A. Samples

In this work we consider microemulsions consisting of water and *n*-decane and nonionic surfactant $C_{10}E_4$ (*n*-decyltetraoxyethylene). To these ternary microemulsions we added amphiphilic block copolymers of the PEP*x*–PEO*y* type, where *x* and *y* denote the molecular weights of each block in kg/mole. These block copolymers have similar structures as $C_{10}E_4$ and differ from it mainly by their size and the methyl side groups of the hydrophobic PEP block.

The PEP–PEO block copolymers were synthesized by anionic polymerization. Some details are given in Appendix A. A more detailed description of the polymer synthesis can be found in Refs. 27 and 28.

Table I displays the characterization of the polymers together with the end-to-end distances of the single polymer blocks, R_w for PEO and R_o for PEP. These values were calculated for homopolymers of the corresponding molecular weights. In case of PEO the radii of gyration were calculated with the help of Refs. 27 and 28 and were transformed into the end-to-end radii, R_e, by multiplication with $\sqrt{6}$. The PEP-block end-to-end radii, R_o, were obtained by the relation $R_o = R_B([\eta]_o/[\eta]_B)^{1/3}$, where R_B is the end-to-end distance in the theta-solvent benzene at 19 °C and was calculated from Ref. 29, and $[\eta]_O$ and $[\eta]_B$ are the intrinsic viscosities in oil and benzene, respectively. For $[\eta]_O$ values in cyclohexane were used instead of decane, as the solvent qualities of cyclohexane and decane are similar for PEP. The molecular weight dependences are $[\eta]_O = 2.81\times10^{-4}M_w^{0.7}$ (Ref. 42) and $[\eta]_B = 2.03\times10^{-3}M_w^{0.5}$ (Ref. 30).

In order to perform experiments under polymer contrast, a fully deuterated $C_{10}E_4$ had to be synthesized. Details are again given in Appendix A. The samples for the structural investigations by small angle neutron scattering (SANS) were prepared using deuterated water (D_2O) and hydrogenous *n*-decane (*h*-decane) for the oil-water or bulk contrast and with D_2O and deuterated *n*-decane (*d*-decane) for the film contrast.

In order to achieve the polymer contrast, microemulsions of D_2O, *d*-$C_{10}E_4$/*h*-$C_{10}E_4$ mixtures, and *d*-decane/*h*-decane mixtures were prepared so that the scattering length densities of surfactant and decane were matched to that of D_2O. Prior

Reuse of AIP Publishing content is subject to the terms: https://publishing.aip.org/authors/rights-and-permissions. Downloaded to IP: 145.94.180.253 On: Thu, 17 Mar 2016 15:06:52

TABLE I. Polymers used as additives.

		PEP–OH		PEP–PEO			
	Composition	M_n/g/mol	M_w/M_n	M_n g/mol	M_w/M_n	R_w/Å	R_o/Å
PEP5–PEO5	*d*6.37h3.63/*h*	5180	1.03	11 100	1.03	77	67
PEP5–PEO15	*h*/*h*	4770	1.03	18 900	1.02	138	67
PEP10–PEO10	*d*6.25*h*3.75/*h*	9880	1.02	21 300	1.02	113	97
PEP22–PEO22	*d*6.61*h*3.39/*h*	23100	1.02	49 000	1.03	181	159

to the preparation of the polymer contrast microemulsions, the *d*-surfactant and the *h*-surfactant were stirred for 24 hours under high vacuum to eliminate adsorbed water. The deuteration degree of the *d*-decane was measured by ^{1}H-NMR as described for the PEP–OH in Appendix A. For D_2O, the value of 99.96% indicated by the manufacturer (Aldrich) was used and the sealed ampoule was first opened prior to the experiments. As the *d*-$C_{10}E_4$ as well as the *h*-$C_{10}E_4$ contained OH end groups which exchange protons with the deuterons of D_2O, this effect was considered for the deuteration degree of D_2O as well as *d*-$C_{10}E_4$. The values are given in Table II. The volume densities of the components were measured with an Anton Paar DMA 5000 density meter. The results for 30.15 °C and the thermal expansion coefficients are also given in Table II. For *h*-$C_{10}E_4$, the value corresponds to the density in the microemulsion and not in the bulk material. To obtain this value, five microemulsions in the one-phase region, containing 14 to 22 wt % surfactant, were measured. With the knowledge of the mass fractions of water, decane, and surfactant as well as the measured densities of bulk water and decane it was possible to calculate the *h*-$C_{10}E_4$-film densities. The value given in Table II is the average value of all five measurements. In order to demonstrate the precision of the measurements it should be noted that no value differed more than 0.02% from the average. The densities of *d*-decane and *d*-$C_{10}E_4$ were calculated from the hydrogenous components taking into account the different molar masses of the *h* and *d* molecules. With the deuteration degrees and the volume densities it was possible to calculate precisely the scattering length densities of the components. These data are also listed in Table II.

In order to characterize the sample compositions, we need three parameters for the quaternary systems. They are defined as $\Phi_\alpha = V_{\text{oil}}/(V_{\text{water}}+V_{\text{oil}})$, the volume fraction of oil in water plus oil, $\Phi_\gamma = (V_{\text{surfactant}}+V_{\text{polymer}})/(V_{\text{water}}+V_{\text{oil}}+V_{\text{surfactant}}+V_{\text{polymer}})$, the overall volume fraction of amphiphile including the polymer, and $\Phi_\delta = V_{\text{polymer}}/(V_{\text{surfactant}}+V_{\text{polymer}})$, the volume fraction of polymer in the mixture of surfactant plus polymer. With the known mass densities given in Table II and $\rho_{\text{polymer}} \simeq 1.0$ g/cm^3, the volume fractions Φ_α, Φ_γ, and Φ_δ quoted in this paper have been derived from the corresponding mass fractions under the assumption of simple additivity on mixing; mass differences due to H/D exchange have been taken into account as appropriate.

A small percentage of the surfactant molecules is solubilized in the water- and oil-excess phases at three-phase coexistence, and similarly in the water and oil domains of a bicontinuous microemulsion.[31] Therefore the surfactant volume fraction Φ_γ is slightly different from the membrane volume fraction Ψ, which has been corrected for this effect.

Table III displays the composition of the samples used in this study. We note that in order to investigate the polymer scattering as well as the polymer-film interference contribution, an array of 15 different contrasts around the theoretical point of zero contrast among oil, water and surfactant were used, as explained in more detail in Sec. II C 5 below.

B. Phase behavior of the microemulsions

At equal volume fractions of water and oil, ternary microemulsions of water, *n*-alkane and C_iE_j as a function of temperature display phase boundaries with a symmetric shape well known as the ''fish'' (solid lines in Fig. 2). At low temperature an oil-in-water microemulsion coexists with an upper oil excess phase (denoted by $\underline{2}$), while at high temperature a water-in-oil phase coexists with a lower water excess phase (denoted by $\overline{2}$). At intermediate temperatures and low surfactant concentrations, a three-phase body appears (upper oil excess phase, middle-phase microemulsion and lower water excess phase, denoted by 3). In the fish tail at intermediate temperatures and somewhat higher surfactant concentrations, a one-phase region occurs (denoted by 1) which relates to a bicontinuous microemulsion.

TABLE II. Densities and scattering length densities of the constituents.

T=30.15 °C	D_2O	*h*-decane	*d*-decane	*h*-$C_{10}E_4$	*d*-$C_{10}E_4$
Degree of deuteration (atom%)	99.71	0.01	98.87	0.01	99.23
Density (g/ml)	1.1031	0.7222	0.8332	0.97047	1.0776
Expansion coefficient (g/ml/°C)	2.7313×10^{-4}	7.604×10^{-4}	8.774×10^{-4}	7.860×10^{-4}	8.619×10^{-4}
Scattering length density [10^{10} cm^{-2}]	6.320	−0.483	6.438	0.180	6.858

Reuse of AIP Publishing content is subject to the terms: https://publishing.aip.org/authors/rights-and-permissions. Downloaded to IP: 145.94.180.253 On: Thu, 17 Mar 2016 15:06:52

TABLE III. Sample compositions for $C_{10}E_4/PEP_{10}$–PEO_{10} microemulsions. (Ψ specifies the membrane volume fraction, i.e., Φ_γ corrected for the $\simeq 2wt\,\%$ surfactant solubility in decane.)

Run No.	α	γ	δ	Φ_α	Ψ	Φ_δ	Φ_γ	Contrast
Sample 15	0.398	0.138	0	0.51	0.127	0	0.127	
Sample 16	0.397	0.106	0.024	0.50	0.095	0.024	0.093	
Sample 17	0.397	0.079	0.051	0.50	0.068	0.053	0.065	Bulk
Sample 18	0.396	0.067	0.074	0.50	0.057	0.079	0.053	
Sample 19	0.396	0.054	0.106	0.50	0.044	0.112	0.040	
Sample 20	0.434	0.127	0	0.51	0.123	0	0.123	
Sample 21	0.432	0.097	0.031	0.51	0.092	0.032	0.089	
Sample 23	0.434	0.065	0.077	0.51	0.058	0.083	0.054	Film
Sample 24	0.434	0.055	0.099	0.51	0.048	0.110	0.043	

The samples were prepared by weighing the masses in test tubes. The tubes were sealed and the occurring phases were observed as a function of temperature. The observation of the phase diagrams was done in a thermostated water bath, where the temperature could be controlled up to 0.02 K. The occurrence of different phases was determined by visual inspection in both transmitted and scattered light. Crossed polarizers were used in order to detect the presence of lamellar phases. We note that the phase diagrams for microemulsions prepared on the basis of D_2O are shifted in temperature by about 2 K to lower values compared to those with H_2O. On the other hand, microemulsions containing d-$C_{10}E_4$, D_2O and *d*-decane are shifted by about 7 K upwards compared to the microemulsions containing hydrogenous materials. However, the fish-tail points stay virtually at the same composition Φ_γ, independently of deuterated or hydrogenous materials.

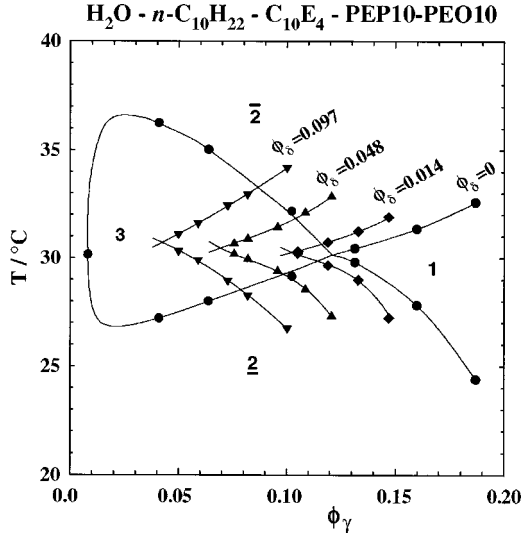

FIG. 2. Three-phase body (3) and adjacent one-phase (1) region for water–*n*-decane–$C_{10}E_4$ containing equal volume fractions of water and decane. Addition of the amphiphilic block copolymer PEP10–PEO10 shifts the one-phase region to smaller surfactant volume fraction Φ_γ. $\underline{2}$ and $\overline{2}$ refer to o/w and w/o microemulsions in equilibrium with their respective excess phases. Φ_δ denotes the volume fraction of polymer in the surfactant.

C. Small angle neutron scattering

1. Data collection

The SANS experiments under bulk and film contrasts were performed at the KWS-1 SANS instrument at the FRJ-2 reactor of the Forschungszentrum Jülich. The experiments were carried out at sample-to-detector distances of $L=1.25$, 5 and 20 m using a neutron wavelength of $\lambda=7$ Å [$\Delta\lambda/\lambda=20\%$ full width at half maximum (FWHM)]. Thereby a Q range of $0.0038\ \text{Å}^{-1}<Q<0.25\ \text{Å}^{-1}$ was covered. Experiments near polymer contrast were carried out at the high intensity SANS diffractometer D22 at the Institute Laue Langevin in Grenoble. Using a wavelength of $\lambda=6$ Å ($\Delta\lambda/\lambda=10\%$ FWHM) and choosing two detector positions $L=2$ and 14 m, D22 covered a Q range of $0.0033\ \text{Å}^{-1}<Q<0.46\ \text{Å}^{-1}$; the geometrical upper limit is reduced to about $0.2\ \text{Å}^{-1}$ because the scattering from our samples dropped below the (incoherent) background beyond this Q value.

All scattering experiments were performed in the one-phase region near the fish-tail point of the phase diagram, where structures are bicontinuous. The samples were equilibrated at the fish-tail point temperatures and filled into Hellma-quartz cells of 0.2 mm optical path length for the bulk-contrast measurements, 1 mm path length for the film-contrast measurement, and 5 mm path length for the polymer contrast, respectively.

A sample thermostat which was able to keep the desired temperatures within 0.02 °C was employed. It could be easily removed in order to check whether the samples stayed in the bicontinuous one-phase region just before and after each measurement by visual inspections in transmitted light.

Each data set was normalized to absolute intensity by the incoherent scattering of H_2O. The data sets from the different detector distances overlapped without scale adjustment.

2. Partial structure factors in ternary and quaternary fluid mixtures

The small angle scattering of neutrons arises from fluctuations of the scattering length densities $\rho_i=(\Sigma_j b_j)/v_i$ where b_j are the scattering length of different atoms in a molecule i and v_i is the volume of the corresponding molecule. Under the assumption of incompressibility and with the definition of one of the molecular species as reference—its scattering length density may be denoted by ρ_s—the coherent scattering cross section per volume is given by

$$I(Q)=\sum_{i,j}(\rho_i-\rho_s)(\rho_j-\rho_s)S_{ij}(Q) \tag{1}$$

with the partial structure factors $S_{ij}(Q)$ (see, e.g., Ref. 32)

$$S_{ij}(Q)=\frac{1}{V}\int_V\langle\phi_i(\mathbf{r})\phi_j(\mathbf{r}')\rangle\exp[i\mathbf{Q}\cdot(\mathbf{r}-\mathbf{r}')]d^3r\,d^3r'. \tag{2}$$

The integration is performed over the sample volume and $\phi_i(\mathbf{r})$ describes the volume fraction of molecule i at a position $\mathbf{r}$. $|\mathbf{Q}|=(4\pi/\lambda)\sin(\Theta/2)$ is the scattering wave number with Θ the scattering angle and λ the neutron wavelength.

Reuse of AIP Publishing content is subject to the terms: https://publishing.aip.org/authors/rights-and-permissions. Downloaded to IP: 145.94.180.253 On: Thu, 17 Mar 2016 15:06:52

For a quaternary microemulsion containing oil, water, surfactant and polymer, the scattering intensity may be described in terms of partial structure factors

$$I(Q)=(\rho_o-\rho_w)^2S_{oo}(Q)+(\rho_f-\rho_w)^2S_{ff}(Q)+(\rho_p-\rho_w)^2S_{pp}(Q)+2(\rho_o-\rho_w)(\rho_f-\rho_w)\times S_{of}(Q)+2(\rho_f-\rho_w)(\rho_p-\rho_w)S_{fp}(Q)+2(\rho_o-\rho_w)(\rho_p-\rho_w)S_{op}(Q), \tag{3}$$

where *o*, *w*, *f*, and *p* indicate oil, water, film, and polymer, respectively. Water has here been used as the reference indicated above. Considering the very low polymer volume fraction in the microemulsion, in general we may neglect the partial scattering functions S_{pp}, S_{fp}, and S_{op}, which are buried under the S_{oo} and S_{ff} contributions in Eq. (1). For $\rho_f=\rho_w$, the scattering intensity $I(Q)$ then reveals $S_{oo}(Q)$, which we call ''bulk contrast.'' On the other hand, for $\rho_o=\rho_w$; $I(Q)=(\rho_f-\rho_w)^2S_{ff}(Q)$. For this ''film contrast'' the experiment reveals information about the surfactant correlations.

The contrast matching method is very powerful, when it is applied to complex many-component systems, because in principle the signal can be restricted to the components we are interested in. If the scattering length densities ρ_w, ρ_o, and ρ_f are precisely matched, then the scattering intensity will be dominated by polymer–polymer partial scattering function $S_{pp}(Q)$, and we may obtain information about the structure of the polymer. This contrast is called ''polymer contrast.''

For the partial structure factors a number of relations can be derived. Let us first consider a ternary microemulsion of oil, water and surfactant. Without the polymer terms, Eq. (3) reduces to

$$I(Q)=(\rho_o-\rho_w)^2S_{oo}(Q)+(\rho_f-\rho_w)^2S_{ff}(Q)+2(\rho_o-\rho_w)(\rho_f-\rho_w)S_{of}(Q). \tag{4}$$

Here water has been used as the reference. When oil is used as the reference, this equation is modified to

$$I(Q)=(\rho_w-\rho_o)^2S_{ww}(Q)+(\rho_f-\rho_o)^2S_{ff}(Q)+2(\rho_w-\rho_o)(\rho_f-\rho_o)S_{wf}(Q). \tag{5}$$

Equations (4) and (5) are equivalent. Therefore, for structures, which are invariant (on average) under an exchange of oil and water, we find

$$S_{ww}(Q)=S_{oo}(Q),\qquad S_{wf}(Q)=S_{of}(Q). \tag{6}$$

Then inserting Eq. (6) into Eqs. (4) and (5), we obtain

$$S_{of}(Q)=S_{wf}(Q)=-\tfrac{1}{2}S_{ff}(Q). \tag{7}$$

Equation (7) agrees with a result derived by Gompper and Schick[33] on the basis of a lattice model for ternary mixtures.

The above discussion can easily be extended to quaternary system. For a quaternary microemulsion with oil, water, surfactant and polymer, the scattering intensity is given by Eq. (3). From the equivalence of water and oil as references for an oil–water symmetric structure, Eq. (6) is amended by $S_{wp}(Q)=S_{op}(Q)$. The same procedure as above then leads to

$$S_{of}(Q)=S_{wf}(Q)=-\tfrac{1}{2}(S_{ff}(Q)+S_{fp}(Q)),\qquad S_{op}(Q)=S_{wp}(Q)=-\tfrac{1}{2}(S_{pp}(Q)+S_{fp}(Q)). \tag{8}$$

Since $S_{ff}(Q)$ is about 10^3 times larger than $S_{fp}(Q)$ for the range of polymer concentrations investigated in this paper, and since $S_{fp}(Q)$ vanishes at high Q, Eq. (7) is almost valid even for a quaternary, oil–water symmetric system.

Finally, we note that the off-diagonal partial structure factors S_{of}, S_{op}, and S_{fp} also contain valuable information; S_{fp}, for example, yields the density profiles of polymers tethered to the surfactant layer—as explained in detail in Sec. III B 4 below.

3. Background subtraction

In the case of the contrast-variation series around the total matching point, the total scattering intensities were very low and particular care had to be taken for the background subtraction. Two origins of the background are considered: first incoherent scattering, and second the coherent scattering caused by mixing of deuterated and hydrogenous materials of one species. In our case, the mixing of *h*-decane/*d*-decane and of h-$C_{10}E_4$/d-$C_{10}E_4$ gives rise to this type of scattering. The incoherent scattering intensity of the system may be calculated to

$$I_{\text{incoh}}=\sum_i \frac{\sigma_i^{\text{incoh}}}{4\pi v_i}\Phi_i, \tag{9}$$

where *i* indicates the *i*th component in the system, and v_i is the volume of the molecule type *i*, σ_i^{incoh} is the incoherent cross section of a molecule of type *i*, i.e., the sum of the incoherent cross sections of its atoms, and Φ_i is the volume fraction of the component *i*, respectively. However, it is commonly experienced that this underestimates the incoherent background level as observed in typical SANS experiments.

To estimate the scattering contributions of *h*-decane and h-$C_{10}E_4$, we assume that the shape of $C_{10}E_4$ in the interface can be modeled by a cylinder; a Debye function, Eq. (12), is used to approximate the form factor of decane. The respective forward scattering is given by

$$I(Q\simeq 0)=\frac{d\Sigma}{d\Omega}(Q)=\Phi(1-\Phi)v\Delta\rho^2, \tag{10}$$

where Φ is the volume fraction of the scattering molecules, v is their molecular volume, and $\Delta\rho$ is the difference of scattering length densities between the protonated scatterer and the average of others: i.e., $\Delta\rho=\rho_{\text{scatterer}}-\overline{\rho}$, where $\overline{\rho}$ is the average except the scatterer. The form factor of a randomly oriented cylinder is given by

$$P(Q)=4\int_0^{\pi/2}\{\sin(QH\cos\beta)/(QH\cos\beta)\}^2\times\{J_1(QR\sin\beta)/(QR\sin\beta)\}^2\,d\beta, \tag{11}$$

Reuse of AIP Publishing content is subject to the terms: https://publishing.aip.org/authors/rights-and-permissions. Downloaded to IP: 145.94.180.253 On: Thu, 17 Mar 2016 15:06:52

where $2H$ is the height of the cylinder and R is the radius of the base. Finally, the Debye function is

$$f_{\text{Debye}}(x)=2\frac{\exp(-x)-1+x}{x^2} \tag{12}$$

with $x=R_g^2Q^2$ and radius of gyration R_g. We used the parameters $2H=10.8$ Å, $R=4.1$ Å as inferred from the geometrical parameters given in Ref. 16, and $R_g=3.0$ Å following from a fit to the Debye function.

After the subtraction of the calculated, Q-independent incoherent scattering and the slightly but significantly Q-dependent coherent scattering from *h*-decane and *h*-$C_{10}E_4$ in their deuterated environment, all corrected data show a plateau in the high-Q region. The actual background levels were obviously about a factor 2 higher, mainly due to the effect of multiple incoherent scattering. We subtracted this average value at high Q as an additional background.

4. Asymptotic behavior

The scattering intensity at large wave vectors Q is well known to be dominated by the contributions of the local interface profile (Porod scattering).[34,16] Under bulk contrast, the scattering intensity is given by

$$I(Q)=2\pi(\rho_0-\rho_w)^2\frac{S}{V}Q^{-4}\exp(-Q^2\Sigma^2), \tag{13}$$

where S/V is the amount of interface per unit volume and Σ is the Gaussian roughness of the interface. Σ originates from the assumption that the scattering-length density profile changes smoothly across the interface, which may be approximated by an error-function shape. The convolution of a step profile with a Gaussian in real space—which leads to the error-function shape—leads to a multiplicative term $\exp(-Q^2\Sigma^2)$ in reciprocal space. If the contrast is known precisely, the specific surface, S/V, can be obtained directly from the scattering intensities.

Under film contrast, only the surfactant sheets contribute to the scattered intensity. We model the small-scale properties of this sheet structure by an ensemble of randomly oriented discs of size L and the thickness t. In this case, the scattered intensity is[35]

$$I(Q)=(\rho_f-\rho_w)^2\Psi\pi L^2\frac{D(QL/2)}{QL/2}\frac{1}{t}\left(t\frac{\sin Qt/2}{Qt/2}\right)^2 \times\exp(-Q^2\Sigma^2). \tag{14}$$

Here, $\Psi=t(S/V)$ describes the volume fraction of the surfactant located at the interface, and

$$D(x)=\exp(-x^2)\int_0^x dt\,\exp(t^2) \tag{15}$$

is the Dawson function. The expression $D(QL/2)/(QL/2)$ originates from the angular averaging of the disc orientation. The last two terms are the form factor of a disc with smooth edges, for wave vectors perpendicular to disc plane. In practice $[\sin(Qt/2)/(Qt/2)]^2\exp(-Q^2\Sigma^2)$ may be replaced by $\exp(-Q^2t_{\text{eff}}^2)$ with $t_{\text{eff}}=\sqrt{t^2/12+\Sigma^2}$, inferring an approximately Gaussian surfactant density as shown in Ref. 36. At large Q, Eq. (14) then takes the form

$$I(Q)=(\rho_f-\rho_w)^2\Psi\frac{2\pi}{Q^2}t\exp(-Q^2t_{\text{eff}}^2). \tag{16}$$

5. Double contrast variation

Polymer scattering may be observed, if the scattering length densities of water, oil and surfactant are matched. Then a single protonated chain in the deuterated environment will give rise to the signal from the individual polymer chains. Since very large intensity differences between the scattering under bulk (order of magnitude 10^5 cm^{-1}), film (10^2 cm^{-1}), and polymer contrast below (1 cm^{-1}) are expected in the investigated range of compositions, small errors in the sample composition will already miss the zero matching point between oil, water and surfactant in a way that the unwanted scattering contributions dominate. Such errors could also occur due to not precisely known degrees of deuteration or densities of the different components.

In order to avoid these difficulties, we performed a two-dimensional contrast variation procedure around the theoretical matching point. As a starting point three samples containing pure D_2O and *d*-decane with three different mixtures of deuterated and a hydrogenated surfactant were prepared. The overall sample composition was a total amphiphile volume fraction $\Phi_\gamma=0.05$ and a polymer fraction in the amphipile $\Phi_\delta=0.096$, resulting in a total polymer content (volume fraction) of 0.0045. As a polymer, a fully hydrogenated PEP5–PEO15 diblock copolymer was used. For each sample a series of studies with a stepwise reduction of the scattering length density of the oil phase were performed by adding minute amounts of *h*-decane (between 6 and 15 mg).

Though the volume of the sample was changed by each addition of *h*-decane, the variation of volume fractions of each component were less than 1 vol %. Therefore, possible structural changes due to this effect could be ignored. The addition of *h*-decane was done with a microsyringe through the tiny hole of the stopper of a cuvette and the mass of additional *h*-decane was checked with a chemical balance. Table IV shows the resulting sample compositions.

Figure 3 displays the scattering length density plane ($\rho_o-\rho_w$ vs $\rho_f-\rho_w$) where the symbols indicate the contrasts chosen for the different experiments. For all 15 contrasts, SANS experiments were performed covering a Q range of $0.0038<Q<0.2$ Å^{-1}.

Figure 4 presents the obtained data sets for the three contrast variation lines. Let us consider, e.g., the series 3H which is closest to the total matching point of oil, water and surfactant. The different intensities relate to the scattering length densities displayed in Fig. 3 from top to bottom. The uppermost data are dominated by the contrast between deuterated water and fully deuterated oil. There at low Q the bulk scattering prevails and the intensity increases by two and one-half orders of magnitude from the intermediate Q inflection point. The two intermediate data sets are obtained close to the total matching point and reveal to a large extent

Reuse of AIP Publishing content is subject to the terms: https://publishing.aip.org/authors/rights-and-permissions. Downloaded to IP: 145.94.180.253 On: Thu, 17 Mar 2016 15:06:52

TABLE IV. Composition of samples of the 2D contrast variation.

Initial composition	D_2O/g	*d*-decane/g	*h*-$C_{10}E_4$/g	*d*-$C_{10}E_4$/g	Polymer/g
2Ha	1.3919	1.0649	0.0000	0.1272	0.0127
3Ha	1.5435	1.1817	0.0096	0.1307	0.0143
4Ha	1.4157	1.0826	0.0166	0.1108	0.0140

Added *h*-decane and corresponding volume fractions of the components

	Total addition of *h*-decane/g	Φ_{D_2O}	$\Phi_{d,h\text{-decane}}$	$\Phi_{d,h\text{-}C_{10}E_4}$	$\Phi_{Polymer}$
2Ha	0.0000	0.4712	0.4800	0.0443	0.0045
2Hb	0.0067	0.4696	0.4818	0.0441	0.0045
2Hc	0.0135	0.4679	0.4836	0.0439	0.0045
2Hd	0.0202	0.4663	0.4854	0.0438	0.0045
2He	0.0270	0.4647	0.4872	0.0436	0.0045
2Hf	0.0343	0.4630	0.4891	0.0435	0.0045
3Ha	0.0000	0.4714	0.4797	0.0443	0.0046
3Hc	0.0150	0.4681	0.4834	0.0440	0.0046
3Hd	0.0226	0.4664	0.4852	0.0438	0.0046
3He	0.0300	0.4648	0.4870	0.0437	0.0046
3Hf	0.0373	0.4633	0.4887	0.0435	0.0045
4Ha	0.0000	0.4713	0.4795	0.0442	0.0049
4Hc	0.0141	0.4680	0.4833	0.0439	0.0049
4Hd	0.0207	0.4664	0.4850	0.0437	0.0049
4Hf	0.0341	0.4633	0.4884	0.0434	0.0049

the polymer scattering which we will discuss later. If we go down further in scattering-length density of the oil, then again the mismatch between water and oil increases and the bulk scattering appears again.

The data sets displayed above were evaluated on the basis of Eq. (3) under the assumption that all contrasts are known from the sample preparation. Equation (3) contains six unknowns and—with the use of the full experimental data set—leads to an overdetermined set of 15 equations for each Q value. These equations were solved by singular-value decomposition, which is equivalent to a least-square fit. In order to improve further the stability of the solution, we introduced the partial scattering functions $S_{oo}(Q)$ and $S_{ff}(Q)$, which are already known from the measurements under film and bulk contrasts. Furthermore, we imposed the condition $S_{of}(Q) = -1/2 S_{ff}(Q)$, compare Eq. (7).

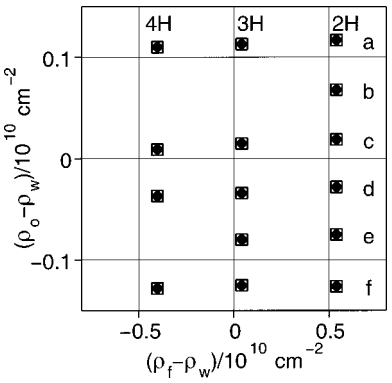

FIG. 3. Location of the samples used for the contrast matching experiment in the scattering length density plane ρ_w, ρ_f.

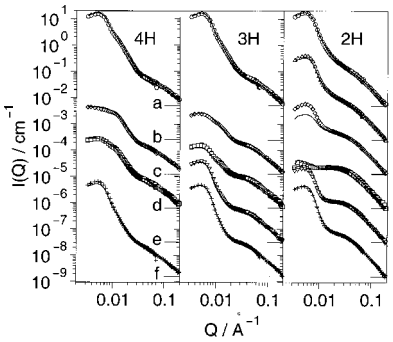

FIG. 4. Scattering intensities obtained for the different contrasts around the 2D matching point. Uppermost curves are scaled by 1 each step down corresponds to an additional scaling factor of 0.05. The level marks $a \cdots f$ indicate the 0.005 cm^{-1} level for each curve. The arrangement of the curves corresponds to the 2D contrast field displayed in Fig. 3. Solid lines represent the reconstructed intensities from the inferred partial scattering functions.

In the next step, we refined the evaluation procedure with respect to the precise location of the overall matching point, a procedure that relies on the external conditions fixing S_{oo}, S_{ff} and S_{of}. For this purpose we calculated the total sum of errors of the backsubstituted solution as a function of the scattering contrast $\rho_o - \rho_w$. This procedure leads to a parabolic dependence on $\rho_o - \rho_w$ with a minimum yielding the new matching point which shifts from 6.32 to 6.28, less than a 1% correction. With this new matching point the evaluation procedure was iterated yielding the final result. The same procedure is, in principle, possible on the $\rho_f - \rho_w$ direction to determine ρ_f. However, unfortunately, the minimum of the least squares error signal as function of $\rho_f - \rho_w$ is too shallow to reliably determine the matching point. This property originates from low intensity of the S_{ff} which is between 2 and 3 orders of magnitude lower than S_{oo}. Therefore it is more reliable to choose the result of ^{1}H-NMR measurement which gives the degree of deuteration and the result of density measurement to determine ρ_f (see Sec. II A and Table II). On the basis of the thus obtained partial structure factors, we reconstructed the scattering intensities of the three contrast variation lines by backsubstituting them into Eq. (4). The reconstructed intensities are included in Fig. 4 as solid lines. A nearly perfect reconstruction is achieved.

This data evaluation procedure leads to the partial structure factors S_{pp}, S_{fp} and S_{op}, see Figs. 5 and 6. While the first two partial structure factors are not too sensitive to slight variations of the oil, water and surfactant contrasts, this is not the case for the polymer–oil interference term. Its form depends crucially on the detailed position of the oil–water matching point and we conclude that this particular structure factor cannot be reliably derived from our experiment.

III. THEORETICAL CONSIDERATIONS

A. Phase behavior

Several levels of theoretical modeling have been used to understand the structure and phase behavior of microemulsions,[17] which range from microscopic lattice models and Ginzburg–Landau theories to interfacial (or

Reuse of AIP Publishing content is subject to the terms: https://publishing.aip.org/authors/rights-and-permissions. Downloaded to IP: 145.94.180.253 On: Thu, 17 Mar 2016 15:06:52

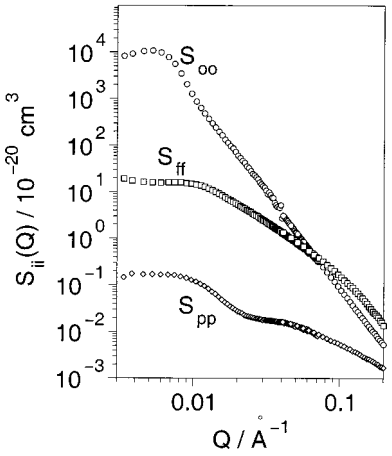

FIG. 5. Partial scattering functions $S_{ii}(Q)$ derived from the data shown in Fig. 4.

membrane) models. In order to understand the effects of amphiphilic block copolymers on the phase behavior, membrane models are most appropriate, in which oil and water are considered as continuum liquids and the interface is treated on a mesoscopic scale as a flexible sheet. For surfactant films being a condensed two-dimensional liquid of molecules, the dominant energy is the bending or curvature energy of the monolayer which can be written as[37,38]

$$H_b = \int dS \left[\frac{\kappa}{2} (c_1 + c_2 - 2c_0)^2 + \bar{\kappa} c_1 c_2 \right]. \tag{17}$$

Here, c_1 and c_2 are the principal curvatures—the inverse principal radii of curvature—at each point of the monolayer, and c_0 is the spontaneous curvature. The bending rigidity κ describes the amount of energy necessary to change the mean curvature away from the spontaneous curvature. The saddle-splay modulus $\bar{\kappa}$ determines the energy cost to create a saddle-type deformation.

Polymers anchored to membranes modify their curvature elasticity. Two regimes have to be distinguished. In the *mushroom regime*—at low polymer density on the membrane—the polymer coils do not interact and fluctuate independently. In this regime, each polymer modifies the curvature elasticity on a membrane patch, the radius of which is proportional to the end-to-end distance of the coil. The effective bending rigidity and the effective saddle-splay modulus therefore should depend *linearly* on the grafting density in this regime.[39–41] At high grafting density, in the *brush regime*, the polymers are stretched away from the membrane due to the repulsive interaction with the neighboring chains. This increases the effect of the polymer on the curvature elasticity, and the dependence on the grafting density is expected to become approximately cubic.[39,42] The crossover between these regimes, the overlap concentration, occurs when the polymer coils just begin to touch, i.e., when the distance between the anchoring points equals the end-to-end distance.

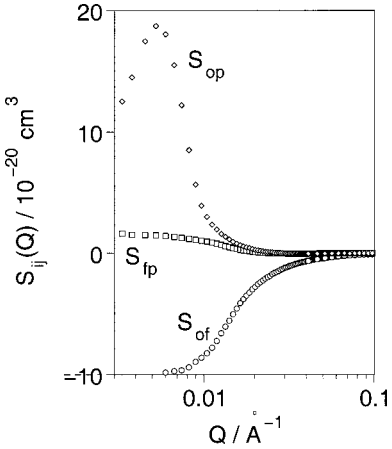

FIG. 6. Partial scattering functions $S_{ij}(Q)$ (cross terms) derived from the data shown in Fig. 4.

The effect of polymer decoration on membrane elasticity in the mushroom regime has already been calculated for ideal chains (without self-avoidance) in Refs. 39–41. For a number density σ of block copolymers within the membrane, the effective curvature moduli $\kappa_{\rm eff}$ and $\bar{\kappa}_{\rm eff}$—which do not contain the renormalization effect due to thermal undulations—can be written in the scaling form

$$\kappa_{\rm eff}(\sigma) = \kappa_0 + \frac{k_B T}{12} \left(1 + \frac{\pi}{2} \right) \sigma (R_w^2 + R_o^2), \tag{18}$$

$$\bar{\kappa}_{\rm eff}(\sigma) = \bar{\kappa}_0 - \frac{k_B T}{6} \sigma (R_w^2 + R_o^2), \tag{19}$$

where κ_0 and $\bar{\kappa}_0$ are the bending moduli of the pure $C_{10}E_4$ membrane, $R_{w,o}^2$ is the mean squared end-to-end distance of the hydrophilic (w) and hydrophobic (o) polymer block (as homopolymers in bulk solution), respectively. These results require some discussion. It is important to note, that they are obtained from a superposition of the effects of independent chains under the assumption that the curvature is distributed uniformly over the whole surface. This is only correct of course, when the mushrooms just begin to overlap. For smaller concentrations, the bending rigidity of the membrane is inhomogeneous. It is well known that two-component mixtures of surfactants or lipids with different spontaneous curvatures but equal bending rigidities actually have a lower effective rigidity than the pure membranes of each component.[43,44] Thus, the bending rigidity in general is a rather complicated function of polymer concentration. In our case, in which we concentrate on the dependence of the fish tail point on the polymer concentration, the spontaneous curvature vanishes, because the microemulsion phase in coexistence with oil- and water-excess phases contains equal amounts of oil and water. Microscopically, the spontaneous curvatures of the surfactant film and of the polymer just cancel at this point, so that even for very asymmetric polymers the spontaneous curvature of the decorated membrane disappears at this point. In this case we can expect Eqs. (18) and (19) to be good approximations also below the overlap concentration $\sigma^* = 1/\max(R_o^2, R_w^2)$. In particular, because polymers evolve on both sides of the membrane, the local deformation[45] of the membrane near the anchoring points of the polymer is negligibly small.

Reuse of AIP Publishing content is subject to the terms: https://publishing.aip.org/authors/rights-and-permissions. Downloaded to IP: 145.94.180.253 On: Thu, 17 Mar 2016 15:06:52

Finally, the anchored polymers could also change the direct interaction of neighboring membranes. This would lead to a steric repulsion due to the confinement of the polymer chains. In the lamellar phase, such an effect has indeed been observed in Ref. 46; near the overlap concentration, it leads to an increase of the effective membrane thickness by the sum of the radii of gyration, R_g, of the two blocks. Note that the end-to-end distance, which appears in Eqs. (18) and (19) is $\sqrt{6}R_g$. Therefore, the increase of the effective membrane thickness should be a minor effect, since the radius of gyration of the polymer coils is somewhat smaller than the size of the oil and water domains already for the system without polymer, and is much smaller near the overlap concentrations. For example, for $C_{10}E_4$, the domain size is about 150 Å without polymer, which increases to about 500 Å near the overlap concentration;[1] this length has to be compared with a radius of gyration of about 60 Å for each block of the longest block copolymer (PEP22–PEO22) we consider.

The phase behavior of an ensemble of interfaces which are modeled as elastic sheets controlled by the curvature energy has been studied intensively in recent years.[17,23,24,47–49] In particular, it has been argued[23,24] that the lamellar phase can only be stable with respect to a proliferation of topological defects, which are passages between neighboring oil or water layers for membrane volume fraction Ψ larger than

$$\Psi \geqslant \Psi^* \exp\left(\frac{2\pi}{\alpha_-}\frac{\bar{\kappa}}{k_B T}\right), \tag{20}$$

where $\alpha_- = 5/3$, and Ψ^* is a constant of the order unity. The form of the instability described by Eq. (20) arises from the effect of thermal short-wavelength fluctuations on the bending moduli κ and $\bar{\kappa}$ on larger length scales. Monte Carlo simulations of randomly triangulated surfaces nicely confirm this picture.[25] Furthermore, the simulations show that the microemulsion coexists with excess oil and water phases along a line which runs almost parallel to the instability line of Eq. (20). A similar result has been obtained in a calculation,[23] in which the free energy of the lamellar phase was approximated by Helfrich's steric confinement expression, and the free energy of the microemulsion phase by the free energy of a minimal surface (of vanishing mean curvature) with a renormalized saddle splay modulus $\bar{\kappa}_R = \bar{\kappa} - (5/6\pi)k_B T \ln(\Psi)$.[50] Combining the results of Eq. (19) and (20) [with $\bar{\kappa}$ replaced by $\bar{\kappa}_{\text{eff}}$ in Eq. (20)], we arrive at the expression

$$\Psi \geqslant \Psi_0 \exp[-\Xi \sigma (R_w^2 + R_o^2)] \tag{21}$$

for the dependence of the amphiphile volume fraction of the microemulsion at the optimal (fish-tail) point on the polymer concentration, where

$$\Xi = \pi/5 \tag{22}$$

and Ψ_0 is the optimal membrane volume fraction of the pure system.

Another interesting quantity, which has been introduced in Ref. 1, is the polymer fraction, $\Phi_{\delta,1/2}$, at the point where the amount of surfactant at three-phase coexistence has been reduced by a factor 2. $\Phi_{\delta,1/2}$ characterizes the efficiency increase due to the addition of block copolymer to a ternary microemulsion. Our result, Eq. (21), for the dependence of the phase boundary on the polymer density, σ, on the membrane implies that this occurs at

$$\Xi \sigma_{1/2}(R_w^2 + R_o^2) = \ln 2. \tag{23}$$

Now, the polymer grafting density σ is related to the volume fraction Φ_δ of polymer in the mixture of both amphiphiles by

$$\sigma = \rho_{\text{polymer}} t N_A M_w^{-1} \frac{\Phi_\delta}{1-\Phi_\delta} \tag{24}$$

as long as the polymer itself has a negligible contribution to the membrane area. In Eq. (24) t is the membrane thickness, M_w the molecular weight of the whole chain, and N_A the Avogadro number. Now, $M_w \sim (N_o + N_w)$, where N_o and N_w are the polymerization indices of the hydrophobic and hydrophilic blocks, respectively. With the usual scaling

$$R_{o,w} = a_{o,w} N_{o,w}^{\nu} \tag{25}$$

with $\nu \simeq 3/5$ for good solvents and $a_{o,w}$ the effective bond lengths of the oil or water soluble polymer blocks, we arrive at

$$\Phi_{\delta,1/2} \propto \frac{N_o + N_w}{a_o^2 N_o^{2\nu} + a_w^2 N_w^{2\nu}}. \tag{26}$$

For symmetric diblocks, where $N_o = N_w \equiv N/2$, Eq. (26) implies, in particular

$$\Phi_{\delta,1/2} \propto N^{1-2\nu} = N^{-1/5}. \tag{27}$$

Therefore, the polymer content, which is required for a given reduction in surfactant concentration, decreases with increasing polymer chain length. Note that this argument is only valid as long as the chains are short enough so that polymers of neighboring membranes have little or no overlap.

B. Theoretical results for the scattering function

1. Bulk and film scattering: Ginzburg–Landau approach

Ginzburg–Landau theories are widely used to describe the thermal behavior near critical points. They also have been applied to ternary microemulsions.[17] In order to describe both the oil–water as well as the surfactant–surfactant correlation functions, two scalar order parameters $\phi(\mathbf{r})$ and $\varphi(\mathbf{r})$ are needed. $\phi(\mathbf{r})$ is identified with the local concentration difference between oil and water whereas $\varphi(\mathbf{r})$ describes the local amphiphile concentration relative to the average concentration $\bar{\varphi}$. Roux *et al.*[18,19] as well as Gompper and Schick[20] calculated the static structure factors due to thermal fluctuations on the basis of such Ginzburg–Landau models. The main difference between these two models is the correlation function $\langle \phi(\mathbf{r})\phi(\mathbf{r}')\rangle$, which is assumed to decay monotonically in Refs. 18 and 19, and to decay with damped oscillations in Ref. 20. We follow here the latter approach, which starts from a free-energy functional,

$$F\{\phi,\varphi\} = F_0\{\phi\} + F_1\{\varphi\} + F_{\text{int}}\{\phi,\varphi\}. \tag{28}$$

Reuse of AIP Publishing content is subject to the terms: https://publishing.aip.org/authors/rights-and-permissions. Downloaded to IP: 145.94.180.253 On: Thu, 17 Mar 2016 15:06:52

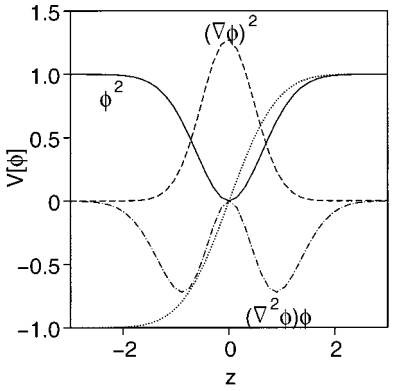

FIG. 7. Sketch explaining the role of the three interaction contributions $V[\phi]$ in the Ginzburg–Landau energy term describing the interaction of the oil/water volume fraction ϕ and the amphiphile fraction φ according to Eq. (31). The dotted line is the assumed shape of $\phi(z)$, z being the coordinate perpendicular to the interface.

Here, F_0 is the well-known Teubner–Strey free-energy functional,[12,17]

$$F_0\{\phi\}=\int d^3r[c(\nabla^2\phi)^2+g_0(\nabla\phi)+\omega_2\phi^2]. \tag{29}$$

F_1 describes the surfactant molecules, which are solubilized in a homogeneous oil or water phase. Their free energy can be modeled by

$$F_1\{\varphi\}=\int d^3r[\alpha(\nabla\varphi)^2+\beta\varphi^2]. \tag{30}$$

Finally, $F_{\rm int}$ describes the interaction between the two order parameters,

$$F_{\rm int}\{\phi,\varphi\}=\int d^3r\,\varphi[\tilde{\gamma}_1\phi^2+(2\tilde{\gamma}_2+\tilde{\gamma}_3)(\nabla^2\phi)\phi + 2\tilde{\gamma}_2(\nabla\phi)^2]. \tag{31}$$

$F_{\rm int}$ has the property of a local chemical potential acting on φ, resulting from the fluctuations of ϕ. The role of the different contributions in $F_{\rm int}$ may be visualized schematically in Fig. 7. The solid curve ϕ^2 depicts the contribution of the first term. If $\tilde{\gamma}_1>0$ then this term will favor smaller than average amphiphile concentration in the bulk phases. The dashed–dotted line $(\nabla^2\phi)\phi$ relates to the contribution of the second term. Provided that the coefficients in front are negative, this contribution will induce smaller than average amphiphile concentrations on both sides of the interface. Finally, the third term, which is depicted by a dashed line $(\nabla\phi)^2$ in Fig. 7, will enhance the amphiphile concentration in the interface if $\tilde{\gamma}_2<0$.

F_0 alone leads to the well-known Teubner–Strey cross section[12] for microemulsions under bulk contrast

$$S(Q)=\frac{8\pi\Phi_o\Phi_w/\xi}{(k^2+\xi^{-2})^2-2(k^2-\xi^{-2})Q^2+Q^4} \tag{32}$$

with $k=2\pi/d$. The scattering intensity (32) is characterized by a pronounced maximum at wave vector $(k^2-\xi^{-2})^{1/2}$. Here, d is the average repeat distance of the water domains and ξ the correlation length. This can be seen most easily from the real-space correlation function,

$$G^0_{\phi\phi}(r)=A\exp[-r/\xi]\frac{\sin(kr)}{kr} \tag{33}$$

with $A=\Phi_o\Phi_w$, which is obtained from Eq. (32) by Fourier transformation.

Similarly, the real-space correlation function for the bulk surfactant reduces to an exponential correlation $G^0_{\varphi\varphi}(r)\propto e^{-r/\xi_\varphi}$ with $\xi^2_\varphi=\alpha/\beta$. The effect of the fluctuations of the order parameter $\phi(\mathbf{r})$ on $G_{\varphi\varphi}$ was calculated by an expansion in the interaction $F_{\rm int}$ to second order in the couplings.[20] The result of this calculation has the form

$$G_{\varphi\varphi}(Q)=G^0_{\varphi\varphi}(Q)+G^0_{\varphi\varphi}(Q)\Gamma\left(Q\xi,\frac{2\pi}{d}\xi\right)G^0_{\varphi\varphi}(Q). \tag{34}$$

The vertex function $\Gamma(x,y)$, a somewhat lengthy expression, is given by Eq. (B8) of Appendix B.

2. Microscopic models of the interaction constants in Ginzburg–Landau theories

The dependence of the coupling constants $\tilde{\gamma}_1$, $\tilde{\gamma}_2$, and $\tilde{\gamma}_3$ on experimental variables like chain length and volume fraction of the block copolymer cannot be understood on the level of the Ginzburg–Landau theory. This requires a more microscopic description of amphiphile self-assembly.

Three-component mixtures can be described in a lattice model by a spin $s_i\in\{0,\pm1\}$ at each lattice site i. If we assign $s_i=0$ to sites occupied by surfactant molecules, and $s_i=+1$ and $s_i=-1$ to sites occupied by water and oil molecules, respectively, then the amphiphilic character of a surfactant molecule can be captured by a 3-spin interaction[17,33]

$$\mathcal{H}_{\rm amph}=\frac{W}{2}\sum_i\sum_\delta s_{i-\delta}(1-s_i^2)s_{i+\delta}, \tag{35}$$

where the second sum runs over all basic lattice vectors from site i to its nearest neighbor sites. In the mean-field approximation, the continuum limit can be made under the assumption that $\langle s_i\rangle$ is a slowly varying function; $\langle s_{i\pm\delta}\rangle$ can then be expanded in a Taylor series, which gives

$$\mathcal{H}_{\rm amph}=\frac{W}{\delta^3}\int d^3r\,\varphi(\mathbf{r})[3\phi(\mathbf{r})^2-\delta^2(\nabla\phi(\mathbf{r}))^2 + \delta^2\phi(\mathbf{r})\nabla^2\phi(\mathbf{r})], \tag{36}$$

where $\phi(\mathbf{r})=\langle s_i\rangle$ and $\varphi(\mathbf{r})=1-\langle s_i^2\rangle$. A comparison with the Ginzburg–Landau model (31) implies

$$\frac{\tilde{\gamma}_3}{\tilde{\gamma}_2}=-4. \tag{37}$$

Other 3-spin interactions, where the three interacting lattice sites do not lie on a straight line, could also be included in the model. In this case, the ratio $\tilde{\gamma}_3/\tilde{\gamma}_2$ is again negative, but now depends on the ratio of the coupling constants W of the

Reuse of AIP Publishing content is subject to the terms: https://publishing.aip.org/authors/rights-and-permissions. Downloaded to IP: 145.94.180.253 On: Thu, 17 Mar 2016 15:06:52

different interactions. We conclude that the lattice model results imply that $\tilde{\gamma}_3/\tilde{\gamma}_2$ should be a negative constant.

The results of the fits of Eq. (34) (see Sec. IV C below) to the experimental data is consistent with a constant, negative value of $\tilde{\gamma}_3/\tilde{\gamma}_2$, as predicted by Eq. (37). The fit also indicates an increase of the absolute values of the coupling parameters $\tilde{\gamma}_1$ and $\tilde{\gamma}_3$ with increasing polymer volume fraction.

A theoretical understanding of this effect could be provided by models, which are similar to those employed for ternary mixtures of *A*-homopolymers of length N_A, *B*-homopolymers of length N_B, and diblock copolymers of length N_{AB}. Such a model for ternary copolymer mixtures has been studied in Ref. 51 for the special case $N_A=N_B=N_{AB}\equiv N$. Although the behavior of this system of equal length polymers is quantitatively certainly quite different from our system of long polymer chains in a short-chain solvent, and also does not contain the dilution effect in the interface due to the surfactant, we believe that we can nevertheless make some qualitative comparison. A Ginzburg–Landau model of the form of Eq. (56) has been derived in Ref. 51, with the result

$$\tilde{\gamma}_1=\frac{1}{(1-\Phi_p)^2}, \tag{38}$$

where Φ_p is the average volume fraction of the block copolymer. Coupling terms with spatial gradients have not been considered, so that no expressions for $\tilde{\gamma}_2$ and $\tilde{\gamma}_3$ are available so far. However, we expect a similar behavior for $\tilde{\gamma}_2$ and $\tilde{\gamma}_3$ as predicted for $\tilde{\gamma}_1$ in Eq. (38), since all three interactions have physically the same effect of attracting the amphiphile to the oil–water interface.

The limiting volume fraction is unity in a ternary mixture of diblock copolymers with two homopolymers. Our system, however, is more complicated. The new feature in the mixture of surfactants and amphiphilic block copolymers is the existence of an overlap concentration Φ_δ^*. Thus, a dependence of $\tilde{\gamma}_1$ as described by Eq. (38) should apply above the overlap concentration. In the mushroom regime, a similar behavior can be expected, but now of the form

$$\tilde{\gamma}_1\sim\frac{1}{(\Phi_\delta^*-\Phi_\delta)^2}. \tag{39}$$

3. Bulk and film scattering: Gaussian-random-field model

Berk,[52,53] Teubner,[54] Pieruschka and Marcelja,[55] and Pieruschka and Safran[21,22] have suggested to model the interfaces in microemulsions as level surfaces of Gaussian random fields. This approach is most useful and predictive, when the Gaussian model of random interfaces is related to the statistical mechanics of microemulsions by a variational approximation.[21,22] Starting point is a Gaussian free-energy functional

$$\mathcal{H}_0[\phi]=\int d^3q\ \nu(\mathbf{q})^{-1}\phi(\mathbf{q})\phi(-\mathbf{q}) \tag{40}$$

very similar to the Ginzburg–Landau free-energy functional (29). However, the spectral density $\nu(\mathbf{q})$ in the functional (40) is now determined by the requirement that the $\phi(\mathbf{r})=0$ level surfaces mimic the behavior of interfaces controlled by the curvature Hamiltonian (17) as well as possible. With such a variational approach, Pieruschka and Safran[21] have been able to relate the parameters in the bulk scattering intensity to the curvature elastic moduli κ and $\bar{\kappa}$.

The film correlation function, $g_{ff}(r)$, can also be calculated for the Gaussian-random-field model. It is found in Ref. 22 to be approximated very well for large r by

$$g_{ff}(r)\approx g_{ff}^{(\infty)}(r) \equiv (S/V)^2+\frac{2}{\pi^2}\left[\tau g(r)^2-\frac{2}{3}g'(r)^2+\frac{1}{9\tau}g''(r)^2\right], \tag{41}$$

where[22,54]

$$\tau=\frac{\langle k^2\rangle}{3}=\left(\frac{\pi}{2}\right)^2\left(\frac{S}{V}\right)^2 \tag{42}$$

and S/V is the amount of interface per unit volume. Here, $g(r)$ is the bulk correlation function,

$$g(r)=\frac{a\xi}{8\pi}\exp[-r/\xi]\frac{\sin(kr)}{kr}, \tag{43}$$

where

$$a=a_0\frac{k_BT}{\kappa}\frac{S}{V},\quad \text{with}\quad a_0=\frac{15\pi^2}{16} \tag{44}$$

which is obtained by a Fourier transformation from the spectral density

$$\nu(q)=\frac{a}{q^4-bq^2+c}. \tag{45}$$

The coefficients b and c in Eq. (45) have been calculated in an expansion in Refs. 21 and 22. It is not too difficult to find also an exact solution, which reads

$$b=2\epsilon\zeta+\frac{\pi^2}{4}\epsilon^2, \tag{46}$$

$$c=\left[\epsilon\zeta+\frac{\pi^2}{4}\epsilon^2\right]^2 \tag{47}$$

with

$$\epsilon=\frac{15}{32}\frac{S}{V}\frac{k_BT}{\kappa},\quad \zeta=\frac{8\pi^2}{5}\frac{S}{V}\frac{\kappa}{k_BT}-\Lambda, \tag{48}$$

where Λ is a high wave-number cutoff, which is contained implicitly in the definition of the Gaussian free-energy functional, Eq. (40), and which is proportional to the inverse size of a surfactant molecule. This implies for the characteristic wave vector k and the correlation length ξ

$$k=\left[\frac{3\pi^2}{16}\epsilon^2+\epsilon\zeta\right]^{1/2}, \tag{49}$$

Reuse of AIP Publishing content is subject to the terms: https://publishing.aip.org/authors/rights-and-permissions. Downloaded to IP: 145.94.180.253 On: Thu, 17 Mar 2016 15:06:52

$$\xi = \frac{4}{\pi}\epsilon^{-1}. \tag{50}$$

For sufficiently large κ, these results reduce to

$$b = \frac{3}{2}\pi^2\left(\frac{S}{V}\right)^2, \quad c = \left(\frac{3\pi^2}{4}\right)^2\left(\frac{S}{V}\right)^4, \tag{51}$$

and

$$k\xi = \frac{64}{5\sqrt{3}}\frac{\kappa}{k_B T}. \tag{52}$$

For small r, on the other hand, Porod's law requires[56]

$$g_{ff}(r) = g_{ff}^{(0)}(r) \equiv \frac{S}{V}\frac{1}{2r}. \tag{53}$$

We combine these two asymptotic results by assuming that the short-range correlation given by Eq. (53) decay exponentially on a length scale which is proportional to the domain size, $d = 2\pi/k$, i.e., we approximate the full film correlation function by

$$g_{ff}(r) = g_{ff}^{(0)}(r)\exp(-\mu k r) + g_{ff}^{(\infty)}(r), \tag{54}$$

where μ is a constant of order unity.

The calculation of the Fourier transform of Eqs. (41) and (54) can be performed without any further approximations. The result of this tedious but rather straightforward calculation is

$$S_{ff}^{(\infty)}(Q) = \frac{1}{8\pi^3}\frac{a^2\xi}{k^2}\left[(\tau\xi^2)I_1(Q\xi,k\xi) - \frac{2}{3}I_2(Q\xi,k\xi) + \frac{1}{9\tau\xi^2}I_3(Q\xi,k\xi)\right], \tag{55}$$

where $I_1 \cdots I_3$ are given in Appendix B. The full scattering function is then given by

$$S_{ff}(Q) = S_{ff}^{(\infty)}(Q) + 4\pi\frac{S}{2V}\frac{\xi^2}{(Q\xi)^2 + \mu^2(k\xi)^2}. \tag{56}$$

The generic shape of $S_{ff}(Q)$ is a $1/Q$ behavior for small Q (but not too small, so that $Q\xi > 1$), followed by a peak or shoulder at $Q = 2k$, and a $1/Q^2$ decay for large Q. By construction, our result (56) reproduces the exact asymptotic scattering intensities for both small and large Q. The intensity in the vicinity of the peak or shoulder is, strictly speaking, beyond the validity of the approximation (56), but captures the main features of the scattering intensity calculated with the (numerically) exact expression for $g_{ff}(r)$.[22] The approximation (56) has the enormous advantage that it can easily be fitted to experimental data, as will be shown in Sec. IV D below. From such fits we find that

$$\mu = 1 \tag{57}$$

works very well; this is the value of μ we use throughout this paper.

4. Polymer-film scattering

Let us assume that the amphiphilic polymer is tethered to the surfactant layer with the hydrophilic PEO part in the water and the hydrophobic PEP part in the oil phase. Figure 8 displays schematically the tethered polymer and its average perpendicular density profile at the interface. For ideal chains, the monomer density, $\phi_p(z)$, of polymers anchored to a planar wall located at $z = 0$ has been calculated exactly in Ref. 57, this situation is illustrated in Fig. 8. In the so-called mushroom regime, it is given by

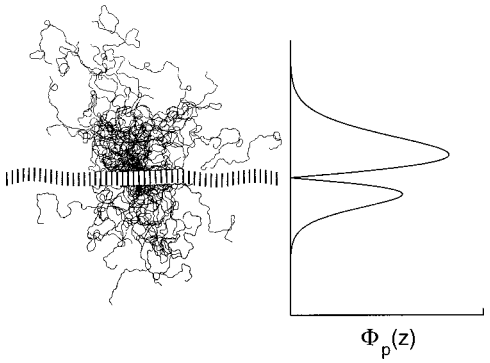

FIG. 8. Schematic picture of the two-sided polymer mushrooms tethered to the amphiphile layer and the corresponding projected densities. For a better graphical representation several polymeric coils have been superimposed.

$$\phi_p(z) = \frac{\sqrt{6\pi}}{R_e}\left[\operatorname{erfc}\left(\frac{1}{2}\sqrt{6}\,\frac{z}{R_e}\right) - \operatorname{erfc}\left(\sqrt{6}\,\frac{z}{R_e}\right)\right] \tag{58}$$

as a function of the distance z from the wall, where R_e is the end-to-end distance of a free polymer chain, and $\operatorname{erfc}(x)$ is the complement of the error function. The real end-to-end distance of an anchored polymer is of course larger than R_e. For ideal chains, the average end-to-end distance *parallel* to the wall is the same as in bulk solution, whereas the anchored polymers are more extended by a factor $\sqrt{2}$ *perpendicular* to the wall.[57] The amplitude in Eq. (58) is defined by the normalization $\int_0^\infty \phi_p(z)dz = 1$. The monomer density vanishes at the wall, has a maximum at $z/R_e = 4\ln 2/(3\sqrt{6}) = 0.377$ and decays exponentially for $z \gg R_e$.

The polymer scattering amplitude is obtained from the one-dimensional Fourier transform of the symmetrized density profile. Due to the simple analytical form of $\phi_p(z)$, this can also be calculated exactly. Thereby we find

$$P(QR_e) = \frac{2\sqrt{6}}{QR_e}\left[D\left(\frac{QR_e}{\sqrt{6}}\right) - D\left(\frac{QR_e}{2\sqrt{6}}\right)\right], \tag{59}$$

where $D(x)$ is Dawson's integral, see Eq. (15).

The partial structure factor $S_{fp}(Q)$, the interference term between polymer and film scattering, follows from the product of the corresponding scattering amplitudes. For an asymmetric PEP–PEO block copolymer with a relative PEP volume fraction f the normalized scattering amplitude from the polymer density is obtained by the (symmetrized) Fourier transformation $P(QR_e)$ of the monomer-density profile, given in Eq. (59),

$$A_p^z(Q) = fP(QR_o) + (1-f)P(QR_w). \tag{60}$$

Reuse of AIP Publishing content is subject to the terms: https://publishing.aip.org/authors/rights-and-permissions. Downloaded to IP: 145.94.180.253 On: Thu, 17 Mar 2016 15:06:52

For a locally flat film of thickness t, the corresponding amplitude is $A_f = \sin(Qt/2)/(Qt/2)$. In order to arrive at $S_{fp}(Q)$, the product $A_f(Q)A_p(Q)$ has to be orientationally averaged over all surface directions within the microemulsion leading to a $1/Q^2$ factor in the high-Q regime similar to Eq. (16).

In the asymptotic Q regime of film scattering $S_{ff}(Q)$ described by Eq. (16), but at not too large Q so that $A_f \simeq 1$, $S_{fp}(Q)$ mirrors directly the (symmetrized) perpendicular polymer density profile

$$S_{fp}(Q) \simeq \frac{1}{Q^2} A_p^z(Q). \tag{61}$$

5. Polymer scattering

The scattering contributions from the tethered polymers may be separated into two parts, (i) the scattering from the average density profile $\phi_p(z)$ and (ii) the diffuse scattering from the correlations of monomers within the chain and possibly among different chains in lateral direction. For infinite planar surfaces, this would be all. For a bicontinuous phase with locally varying curvature, we have to consider further the correlations of the polymers mediated by the tethering to the surfactant film.

The polymer–polymer partial structure factor $S_{pp}(Q)$, which arises from the polymer-decorated surfactant layer, may be written as

$$S_{pp}(Q) = \mathcal{N} S_{ff}(Q) \{A_p^z(Q)\}^2 + \tilde{S}_{pp}(Q). \tag{62}$$

The first term describes the scattering from the surfactant film $S_{ff}(Q)$ with a normalization factor $\mathcal{N}$ related to the decoration density. The polymer density profile gives rise to a form factor $\{A_p^z(Q)\}^2$, which is the square of the respective scattering amplitude. $\tilde{S}_{pp}(Q)$ results from the monomer-density fluctuations discussed above.

In order to illustrate this point, we take the scattering from an ideal coil as an example. In this case, $\tilde{S}_{pp}$ arises from the difference between the Debye function, Eq. (12), which includes all correlations, and the Guinier function $\exp(-Q^2R_g^2/3)$, which is proportional to the squared Fourier transform of the average density profile within the coil with the radius of gyration R_g.

The proper normalization of Eq. (62) may be inferred as follows. Since the monomer density has been normalized in Sec. III B 4 to the number of polymers, $\int dz\, \phi_p(z) = 1$, we have $\lim_{Q\to 0} A_p^z(Q) = 1$, so that $A_p^z(Q)$ just describes the form factor of the polymer layer. $S_{ff}(Q)$ denotes the scattering from a surfactant layer with an area density proportional to Φ_γ/S. Condensing the polymer (visible only under polymer contrast) into that interface yields an area density proportional to $\Phi_\delta\Phi_\gamma/S$. Multiplication of $S_{ff}(Q)$ with $A_p^z(Q)^2$ accounts for the larger extension of the polymer layer compared to the pure amphiphile film. Note, however, that the low-Q intensity remains unchanged by this ''swelling.'' In real space this multiplication relates to a convolution. The remaining normalization is just the square of the ''dilution factor'' given by the relative amount of polymer in the surfactant $\mathcal{N} = \Phi_\delta^2 \simeq 10^{-2}$.

TABLE V. Surfactant/polymer relative amounts at the fish-tail points. Φ_δ, volume fraction of polymer in total amphiphile; Ψ, membrane volume fraction; Φ_γ, total amphiphile volume fraction.

Polymer	Φ_δ	Ψ	Φ_γ
-	0.0000	0.1139	0.1207
PEP1–PEO1	0.0191	0.1060	0.1151
PEP1–PEO1	0.0492	0.0741	0.0854
PEP1–PEO1	0.0781	0.0554	0.0679
PEP5–PEO5	0.0142	0.0901	0.0985
PEP5–PEO5	0.0477	0.0646	0.0754
PEP5–PEO5	0.1148	0.0164	0.0270
PEP10–PEO10	0.0138	0.0929	0.1013
PEP10–PEO10	0.0477	0.0567	0.0671
PEP10–PEO10	0.0961	0.0292	0.0406
PEP22–PEO22	0.0054	0.1039	0.1114
PEP22–PEO22	0.0145	0.0882	0.0967
PEP22–PEO22	0.0289	0.0733	0.0828
PEP22–PEO22	0.0571	0.0439	0.0543
PEP22–PEO22	0.1000	0.0168	0.0270

IV. EXPERIMENTAL RESULTS AND DISCUSSION

A. Phase diagrams

For a variety of polymer-in-amphiphile volume fractions Φ_δ and molecular weights of the diblock copolymers, the phase diagrams around the fish-tail point in the one-phase region were studied. Figure 2 displays results for different polymer contents in a symmetric $C_{10}E_4$ decane/water microemulsion. The fish-tail point without the polymer is observed at $\Phi_\gamma^{(0)} = 0.121$, a value which decreases dramatically by adding the PEP10–PEO10 diblock copolymer, e.g., for $\Phi_\delta = 0.096$, $\Phi_\gamma = 0.041$ is found at the fish-tail point.

All results for the fish-tail or optimal point and for various polymer sizes are compiled in Table V. There, for equal volume fractions of oil and water, Φ_γ and Φ_δ are given together with the size of the block copolymer used.

These results allow for an experimental test of Eq. (21), which predicts an exponential relation between the position of the optimal point and the saddle-splay modulus $\bar{\kappa}$. Equation (21) together with Eq. (19) relates the change in $\bar{\kappa}$ induced by the anchored polymer to the number density of the polymer in the surface and the end-to-end distances R_w^2 and R_o^2 on the water and the oil side, respectively. Figure 9 displays a logarithmic plot of the membrane volume fraction Ψ at the optimal point vs $\sigma(R_w^2 + R_o^2)$. The data for the PEP–PEO block copolymers with four different chain lengths fall onto a single straight line confirming thereby the scaling form of Eq. (21). This result provides evidence that the effect of the polymer is indeed to modify the saddle-splay modulus of the membrane. The slope is found to be

$$\Xi = 1.54 \pm 0.05 \tag{63}$$

roughly twice as large as the theoretical estimate. Since $\Xi = \pi/5$ for ideal chains, we may infer that self-avoiding chains appear to have a more pronounced effect on the saddle-splay modulus than the ideal chains. Figure 9 also shows that the highest polymer number densities are already quite close to the overlap concentration which is located at $\sigma(R_w^2 + R_o^2)$ between 1 and 2. The limiting cases correspond

Reuse of AIP Publishing content is subject to the terms: https://publishing.aip.org/authors/rights-and-permissions. Downloaded to IP: 145.94.180.253 On: Thu, 17 Mar 2016 15:06:52

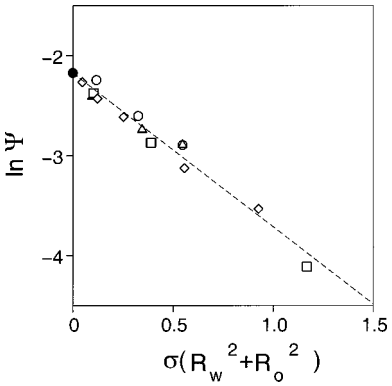

FIG. 9. Logarithm of the membrane volume fraction at the fish tail point as a function of polymer surface coverage. Full circle, no polymer; open circles, PEP1–PEO1; triangles, PEP5–PEO5; squares, PEP10–PEO10; and diamonds, PEP22–PEO22. A linear relation is observed as predicted by Eq. (21).

to strongly asymmetric and symmetric block copolymers, respectively. At the overlap point it is expected that Eqs. (18) and (19) cease to be valid because the brush regime is entered.

Figure 10 displays the dependence of $\Phi_{\delta,1/2}$ on $M_w/(R_o^2+R_w^2)$ for which a linear relation follows directly from a combination of Eqs. (23) and (24). With the assumption of such a linear dependence a slope—from the line through the data—of $\Xi=1.51\pm0.15$ is obtained, which is very close to, but less accurate than that inferred from the data in Fig. 9.

B. Results under bulk contrast

SANS data under bulk contrast have been taken on five different samples of symmetric D_2O/*h*-decane mixtures containing different amounts of surfactant and polymer such that always the fish-tail point was realized (samples 15 to 19 from Table III). Figure 11 displays the synopsis of the SANS data. All structure factors are characterized by a plateau at low Q, a peak at intermediate Q and a Q^{-4} high-Q flank. With decreasing overall surfactant volume fraction—made accessible by increasing the polymer concentration Φ_δ—the scattering curves are displaced to lower Q and at the same time gain intensity. Furthermore, the peak appears to sharpen. The data immediately reveal an increasing domain size $d\simeq 2\pi/Q_{\max}$ with increasing polymer volume fraction. The SANS data were fitted with Eq. (32) extracting thereby both the domain size d as well as the correlation length ξ. The results are listed in Table VI.

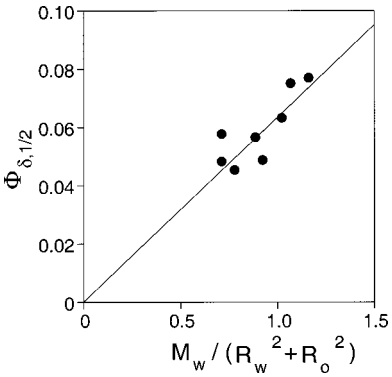

FIG. 10. $\Phi_{\delta,1/2}$, the amount of polymer—corrected for surfactant solubility—in the surfactant layer that is needed to decrease the necessary amount of surfactant by a factor of 2 as a function of the effective surface density of a pair of block copolymer coils. The relation may be inferred from Eqs. (23) and (24). Due to the difficulty of the determination of $\Phi_{\delta,1/2}$ by visual detection of the phase transition the points are somewhat scattered.

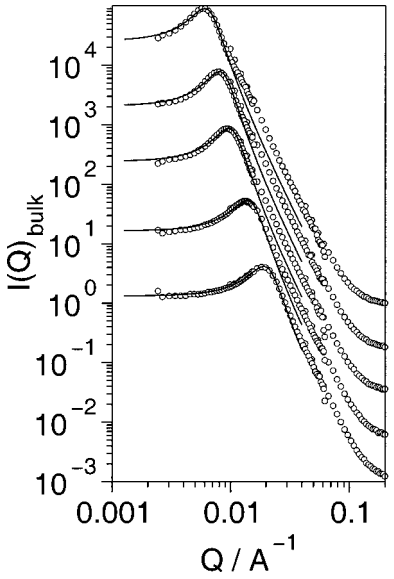

FIG. 11. Bulk contrast SANS data from bicontinuous microemulsion phases close to the fish-tail point (samples $15\cdots19$). The curves correspond to different polymer content in the surfactant Φ_δ and as a consequence different decreasing total surfactant content Φ_γ. From above the values are $(\Phi_\gamma,\Phi_\delta)=(0.045, 0.101)$; (0.060, 0.070); (0.072, 0.048); (0.100, 0.023); and (0.133, 0.000). The curves are separated from each other by a shift factor of 5, the intensity scale applies directly to the uppermost curve. Symbols indicate the data, solid lines indicate fits with the Teubner–Strey form.

Figure 12 presents a plot of the domain size vs the correlation length. While for a large number of microemulsions without polymers, experimentally a value $d/\xi\simeq 2$ is found, adding polymer leads to a gradual decrease of this ratio which assumes a value around 1.8 for larger polymer volume fractions. This decrease indicates that the addition of polymer leads to a gradual ordering of the domains.

In order to obtain information about the membrane, Fig. 13 presents Porod plots of the measured intensities ($\ln[I(Q)Q^4]$ vs Q^2) displaying the asymptotic regime as described by Eq. (13). From fitting the data in the asymptotic regime of these plots, both the specific interface area S/V as well as the interface roughness Σ may be determined. The

TABLE VI. Fit parameters of Ginzburg–Landau theory. The values of d, respectively k, have been determined by interpolation of results from Teubner–Strey fits [to Eq. (32)] of bulk contrast data and were kept fixed in the film contrast fits.

Run No.	ξ Å	d Å	$k=2\pi/d$ (Å^{-1})	ξ_φ (Å)	$\tilde{\gamma}_1$	$\tilde{\gamma}_3/\tilde{\gamma}_2$	$\tilde{\gamma}_3\times10^3$
Sample 20	165	323	0.0194	8.5	0.074	−2.15	0.36
Sample 21	227	439	0.0143	12.7	0.070	−2.32	0.50
Sample 23	375	676	0.0093	18.0	0.156	−2.44	1.83
Sample 24	451	805	0.0078	22.1	0.379	−2.60	6.64

Reuse of AIP Publishing content is subject to the terms: https://publishing.aip.org/authors/rights-and-permissions. Downloaded to IP: 145.94.180.253 On: Thu, 17 Mar 2016 15:06:52

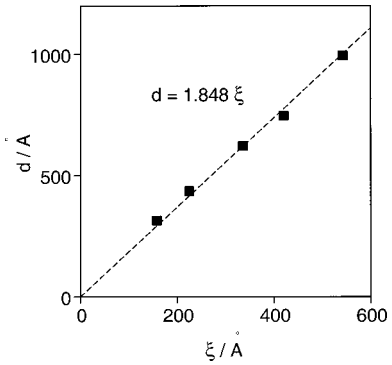

FIG. 12. Domain size d vs correlation length ξ.

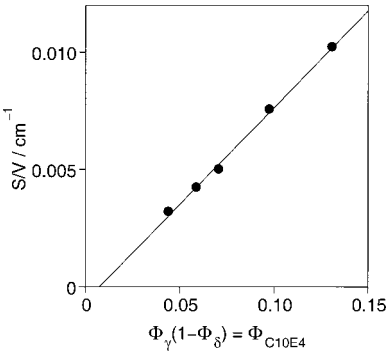

FIG. 14. Specific membrane area S/V corresponding to the fit results shown in Fig. 13 as determined by the Porod analysis as function of the surfactant volume fraction $\Phi_\gamma(1-\Phi_\delta)$.

lines in Fig. 13 correspond to the fits, the jumps at change of detector distance are due to resolution effects. For a quantitative evaluation of S/V it is necessary to know precisely the contrast $(\rho_o-\rho_w)$. The roughness Σ is obtained from the slope of the asymptotes, the specific interface area S/V is evaluated from the absolute value of the prefactor. S/V decreases with increasing polymer volume fraction and Σ amounts to approximately 2 ± 0.3 Å for all samples.

To avoid uncertainties in the range of several percent that may be caused by the errors involved in the absolute calibration of the SANS instruments, for the Porod analysis the corresponding contrast (intensity) factor has been determined by the following procedure. For isotropically disordered two-component systems, the scattering contrast may be calculated by an integration over the measured intensities

$$\int_0^\infty I(Q)Q^2\,dQ=\Phi_d\Phi_h(\rho_d-\rho_h)^2, \tag{64}$$

where Φ_d and Φ_h denote the volume fractions of the hydrogenated and deuterated components and $\rho_{d,h}$ their scattering length densities, respectively. Table VII includes the experimental results following from the integration, Eq. (64), as well as theoretical expectations according to the right-hand side of Eq. (32). As may be seen both numbers agree better than within 10%. With the contrasts inferred from Eq. (64) which automatically also contain a calibration correction, in place, now the specific interface area may be evaluated from Eq. (13) with an accuracy between 2% and 6%. The resulting values are quoted in Table VII. Figure 14 displays the specific interface area as a function of surfactant volume fraction $\Phi_\gamma(1-\Phi_\delta)$—the polymer content which is included in the total surfactant volume fraction has been taken out because the polymer is not supposed to contribute significantly to the membrane area. A linear relationship is found which extrapolates to $S/V=0$ for $\Phi_\gamma=0.0068$. Considering the solubility of 0.02 mass fraction of the surfactant in oil and 0.002 in water, the experimental value agrees very well with a total added surfactant plus polymer volume fraction $\Phi_\gamma=0.0075$ which would be expected from these solubilities to stay in the bulk oil (water) phases and therefore does not contribute to the interface area. Finally, with the result of Fig. 14 and the surfactant density of $\rho_s^m=0.97$ g/cm^3 the thickness of the surfactant layer, may be calculated to $t=\Phi_\gamma(S/V)=12\pm0.2$ Å, slightly less than the length of 16 Å of a straightened $C_{10}E_4$ molecule.

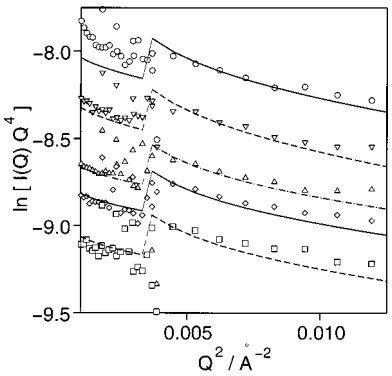

FIG. 13. Porod plot of the data shown in Fig. 11. The dependence of the surface-to-volume ratio S/V from the surfactant content Φ_γ is clearly visible. The interface ''roughness'' gives rise to the slope of the lines representing Eq. (13) and amounts to about 2 Å. The incoherent background has been determined by fitting including the high-Q asymptotically constant level and has been subtracted. The jump in the data and fitted curves at detector distance changes results from the difference in resolution.

C. Results under film contrast

In order to study the relation between the film and the bulk scattering as discussed in the theoretical section, we prepared a series of microemulsions under film contrast with compositions as close as possible to those investigated under bulk contrast (see Table III). Since all microemulsions were studied close to the fish-tail point, increasing the polymer volume fraction leads to a reduction of the overall surfactant concentration Φ_γ because the fish tail is shifting. Figure 15 displays experimental results obtained for different polymer surfactant compositions. The data traces are composed by a low-Q plateau, which crosses over to a high-Q asymptotic $1/Q^2$ behavior as discussed in Sec. III. With increasing polymer concentration, the knee which is the crossover from the low to the high-Q regime shifts towards lower Q in accordance with what is seen for the bulk data.

The experimental results were fitted with both the Ginzburg–Landau approach as well as the random interface model. In each case, the structural lengths d and ξ which were already obtained from the bulk-contrast samples were fixed—the actually used values of d and ξ for film contrast were found by interpolation in order to correct for the small

Reuse of AIP Publishing content is subject to the terms: https://publishing.aip.org/authors/rights-and-permissions. Downloaded to IP: 145.94.180.253 On: Thu, 17 Mar 2016 15:06:52

TABLE VII. Data on contrasts $\langle \eta^2 \rangle = \Phi_h \Phi_d (\rho_h - \rho_d)^2$, the structural lengths, d and ξ, the specific interface area S/V and interface roughness Σ.

		TS			Porod		
	$\langle \eta^2 \rangle_{cal}/cm^{-4}$	$\langle \eta^2 \rangle/cm^{-4}$	d/Å	ξ/Å	$\langle \eta^2 \rangle/cm^{-4}$	$S/V/Å^{-1}$	Σ/Å
Sample 15	10.662×10^{20}	10.219×10^{20}	314	162	11.652×10^{20}	0.010 24	1.9
Sample 16	10.830×10^{20}	9.655×10^{20}	436	229	11.951×10^{20}	0.007 59	2.0
Sample 17	11.009×10^{20}	9.892×10^{20}	629	350	12.077×10^{20}	0.005 03	1.7
Sample 18	11.071×10^{20}	9.925×10^{20}	755	432	12.921×10^{20}	0.004 25	1.7
Sample 19	11.153×10^{20}	10.186×10^{20}	1003	553	13.382×10^{20}	0.003 22	1.8

discrepancies in composition. The dashed lines in Fig. 15 display the result of a fit with the Ginzburg–Landau approach of Ref. 58. As may be seen, in general a very good agreement between theory and experiment has been obtained. The resulting parameters are presented in Table VI. They display a systematic variation with polymer content, which can be compared with the prediction of the lattice model, described in Sec. III B 2. There a relation of $\tilde{\gamma}_3/\tilde{\gamma}_2 = -4$ was predicted, about twice as large as the experimental value. The fits yield a tendency of $\tilde{\gamma}_1$ to increase with the polymer content Φ_δ in the amphiphile, in qualitative agreement with Eq. (39).

In order to fit the film-scattering data to the Gaussian-random-field result (compare Sec. III B 3), we modify Eq. (55) slightly to include the form factor $P(Q)$ of the amphiphile film, so that

$$I(Q) = a_1 \frac{\xi}{k^2}\left[(\tau\xi^2)I_1 - \frac{2}{3}I_2 + \frac{1}{9\tau\xi^2}I_3\right] + a_2\left\{\frac{\xi^2}{(Q\xi)^2 + \mu^2(k\xi)^2}\right\}P(Q), \tag{65}$$

where $I_1 \cdots I_3$ are given in Appendix B and

$$P(Q) = \left(\frac{\sin(Qt/2)}{Qt/2}\right)^2 \exp(-\Sigma^2 Q^2). \tag{66}$$

With that the amplitudes in the above expression may be rewritten as

$$a_1 = \frac{a_0^2}{8\pi^3}\left(\frac{k_B T}{\kappa}\right)^2\left(\frac{S}{V}t\right)^2 \Delta\rho^2 \tag{67}$$

and

$$a_2 = 2\pi \frac{S}{V} t^2 \Delta\rho^2, \tag{68}$$

where t relates to the molecular length ($t = 11-12$ Å) and $\Delta\rho$ is the surfactant-solvent scattering length density difference. A value of $\Delta\rho = 6.39\times10^{10}$ cm^{-2} is used throughout the current analysis. The resulting $\Sigma \simeq 1.1$ Å is a measure of the roughness of the interfaces due to protrusion of the surfactant molecules on atomic scales. This is somewhat smaller than $\Sigma \simeq 2$ inferred from the Porod analysis. However, both values indicate a locally very smooth interface.

Figure 15 presents the comparison of the film-contrast data with the Gaussian-random-field results (solid lines) as expressed by Eq. (65). Table VIII contains the results for the fitting parameters (τ, a_1, a_2, Σ) for the Gaussian random field model and $(\alpha, \xi_\varphi, \tilde{\gamma}_1, \tilde{\gamma}_2, \tilde{\gamma}_3)$ for the Ginzburg–Landau model fits, for which the range was limited to $q_{max} < 4\times 2\pi/d$. Both a_1 and a_2 display the dependencies on the membrane volume fraction $\Psi = t(S/V)$ predicted by Eqs.

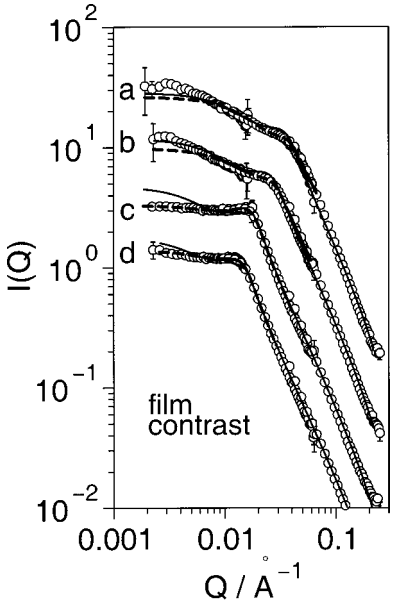

FIG. 15. SANS data obtained under film-contrast and fits. Open symbols are the experimental points, (a) $C_{10}E_4$+PEP10–PEO10 ($\Phi_\delta = 0$); (b) $C_{10}E_4$+PEP10–PEO10 ($\Phi_\delta = 0.032$); (c) $C_{10}E_4$+PEP10–PEO10 ($\Phi_\delta = 0.083$); and (d) $C_{10}E_4$+PEP10–PEO10 ($\Phi_\delta = 0.110$). The intensity scale applies directly to (a). (b)–(c) are successively shifted by a factor of 0.3. Solid lines correspond to fits with the Gaussian random field expression, Eq. (65), dashed lines stem from fits with the Ginzburg–Landau theory, Eq. (34).

TABLE VIII. Fit parameters of Gaussian random field theory.

Run No.	τ $\times10^{12}$ (cm^{-2})	a_1/Ψ^2 $\times10^{-2}$ (cm^{-1})	a_2/Ψ (cm-1)	κ/k_BT	κ_0/k_BT
Sample 20	0.661	0.287	0.131	0.70	1.20
Sample 21	0.355	0.303	0.135	0.66	1.24
Sample 23	0.168	0.334	0.143	0.60	1.30
Sample 24	0.156	0.332	0.146	0.58	1.33

Reuse of AIP Publishing content is subject to the terms: https://publishing.aip.org/authors/rights-and-permissions. Downloaded to IP: 145.94.180.253 On: Thu, 17 Mar 2016 15:06:52

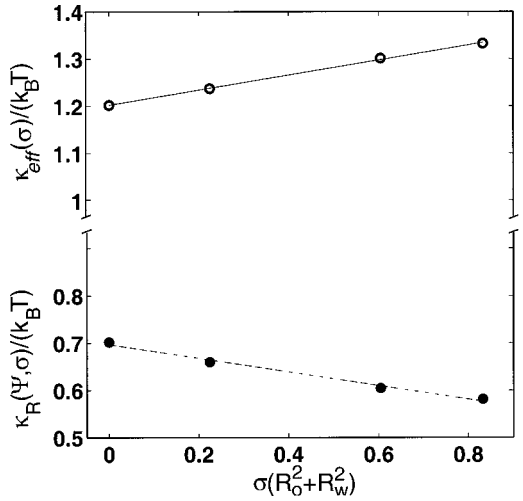

FIG. 16. The estimated bending moduli $\kappa_R(\Psi,\sigma)$ (lower half) and $\kappa_{\text{eff}}(\sigma)$, bare (upper half), determined from fit and Eqs. (67) and (69).

(67) and (68), i.e., $a_1 \sim \Psi^2$ and $a_2 \sim \Psi$. Also τ shows the predicted quadratic dependence on Ψ. From the value of a_1, the bending rigidity κ may be calculated based on Eq. (67). Our results are presented in Table VIII and Fig. 16. They show a rather weak dependence of κ on the polymer grafting density, with a tendency to decreasing values with increasing polymer density.

The value of κ, which is obtained in this way, requires some discussion. First, if should be noticed that the scattering intensity at small wave vectors is sensitive to the exact form of the film–film correlation function, $g_{ff}(r)$, for *all* distances r. Since in our derivation of the film-scattering intensity, we have interpolated between the asymptotic behavior of $g_{ff}(r)$ for small and large r, the values of $S_{ff}(Q)$ in Eq. (56) for small Q do depend on our approximations. Second, the fit value of a_2 in Eq. (65) is determined by the large-Q part of the scattering data—which is just the Porod law —while the fit value of a_1 is determined by the low-Q part. Therefore, the value of κ extracted from Eq. (67) is also sensitive to the approximations made in deriving the analytical expression for $S_{ff}(Q)$. Third, the observations that the fitted a_1 values show the predicted dependence on Ψ and that the extracted κ values fall into the same range of 0.5 to $1.0k_BT$ as observed by several other experiments[59,60] on microemulsion systems, are more indications that we have found a reliable analytical expression for $S_{ff}(Q)$.

Keeping these caveats in mind, we can now proceed to interpret our results for the bending rigidity. The bending rigidity we extract from the scattering intensity at small Q has to be considered as a renormalized quantity, which is affected by the thermal membrane fluctuations on scales smaller than the average domain size. This effect is not described correctly in the Gaussian-random-field approach, and therefore has to be added explicitly. A field-theoretic calculation of membrane fluctuations gives the result[61,62] for the dependence of the renormalized bending modulus κ_R on the polymer coverage σ and the membrane volume fraction Ψ,

$$\kappa_R(\sigma,\Psi) = \kappa_{\text{eff}}(\sigma) + k_BT\frac{3}{4\pi}\ln(\Psi), \tag{69}$$

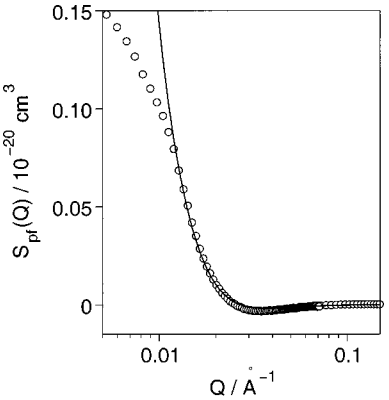

FIG. 17. Partial scattering function $S_{fp}(Q)$ (circles). The line corresponds to a fit to Eq. (61) yielding $R_{\text{PEO}}=161$ Å and $R_{\text{PEP}}=80.5$ Å for PEP5–PEO15. Since Eq. (61) is only valid in the high-Q region fits were performed to data in the Q-range $0.012 \leqslant Q/\text{Å}^{-1} \leqslant 0.2$.

where $\kappa_{\text{eff}}(\sigma)$ denotes the bare bending modulus of the decorated membrane. The renormalized bending rigidity decreases with increasing domain size, i.e., with decreasing membrane volume fraction Ψ. Thus, in order to see the dependence of the (effective) bending rigidity on the polymer concentration, we calculate $\kappa_{\text{eff}}(\sigma)$ from Eq. (69) by identifying $\kappa_R(\sigma,\Psi)$ with the values obtained from the fit of the film-scattering intensity. The result is also shown in Fig. 16. It can be seen that $\kappa_{\text{eff}}(\sigma)$ is a linear function of $\sigma(R_w^2 + R_o^2)$, consistent with the prediction (18). Furthermore, a slope of 0.16 is found, which compares quite well with the theoretical value of $(1+\pi/2)/12 = 0.214$, which is strictly valid only for ideal chains.

D. Measurements under polymer contrast

The partial scattering functions $S_{fp}(Q)$ and $S_{pp}(Q)$ contain information about the used PEP5–PEO15 block-copolymer. $S_{fp}(Q)$ is in particular sensitive to the projection of the average polymer density on the (local) normal direction to the interface. Any fluctuating segment-film correlations average to zero.[63–65] Whereas the latter statement stays valid for the curved interface of the bicontinuous structure the projection property is only valid in the high-Q limit where Eq. (61) approximately holds. There it may be used to determine the extension of the tethered polymer coils on both sides of the interface with the assumption of the density profile, Eq. (58). The $S_{fp}(Q)$ data and fits to Eq. (61) are shown in Fig. 17. The lines display Eq. (61) computed with $R_{\text{PEO}} = 161$ Å and $R_{\text{PEP}} = 80.5$ Å. For the fit procedure, the ratio $R_{\text{PEP}}/R_{\text{PEO}}$ was kept fixed. The fact that the data quickly approach zero at the high-Q end corroborates the expectation that segment-film correlations are not seen in this partial scattering function.

These values should be compared with the end-to-end distances of the corresponding homopolymers in solutions, which have been found to be $R_{\text{PEP}} = 67$ Å (in cyclohexane)[30] and $R_{\text{PEO}} = 138$ Å.[66] Since an error estimate of about 10% is not unreasonable in both types of measurements, we can conclude that the polymer coils behave as isolated, self-avoiding chains, which are neither attracted to the membrane nor compressed by other polymers.

Reuse of AIP Publishing content is subject to the terms: https://publishing.aip.org/authors/rights-and-permissions. Downloaded to IP: 145.94.180.253 On: Thu, 17 Mar 2016 15:06:52

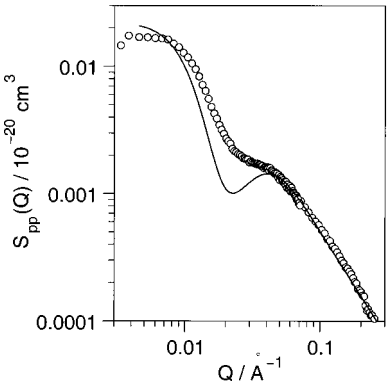

FIG. 18. Partial scattering function $S_{pp}(Q)$. Lines correspond to fits with Eq. (62), the assumed end-to-end radii correspond to the values obtained from the fit shown in Fig. 17. The polymer fluctuation contribution $\tilde{S}_{pp}(Q)$ is modeled by a Beaucage function Eq. (70) with a $Q^{-\nu}$ asymptote ($\nu = 1.66$) and crossover lengths equal to the end-to-end radii.

The polymer–polymer scattering function contains both contributions due to the average polymer density and contributions due to fluctuating segmental correlations. The average density decorates the interface and is expected to be proportional to the film–film scattering multiplied by a polymer form factor as expressed in the first term of Eq. (62). Figure 18 shows $S_{pp}(Q)$ with fits to Eq. (62), the values of the end-to-end radii correspond those obtained from the fit to $S_{fp}(Q)$ (Fig. 17). The polymer fluctuation contribution $\tilde{S}_{pp}(Q)$ is modeled by the fluctuation part of a Beaucage function[67]

$$\tilde{S}_{pp}(Q) \propto (\mathrm{erf}[w(QR_g)/\sqrt{6}]^3/(QR_g))^{\nu} \tag{70}$$

with a $Q^{-\nu}$ asymptote (with $\nu \simeq 5/3$) and crossover length $\sqrt{6}R_g$ equal to the end-to-end radii and $w = 1.06$. The inferred normalization factor $\mathcal{N} = 0.0134$ is slightly larger than the estimate $\mathcal{N} \simeq \Phi_{\delta}^2 \simeq 0.0106$, see Sec. III B 5.

The deviations (missing intensity) at intermediate Q most probably results from the neglect of lateral density fluctuations that result from the average density variation from the center to the periphery of a polymer mushroom if projected onto the oil–water interface. The arrangement of mushrooms tethered to the interface resembles a 2D soft-sphere fluid, the lateral correlation due to its structure factor would at least account for a fraction of the missing intensity. In addition, the used ansatz leading to the first term of Eq. (62) assumes flat interfaces which is only valid in the limit of small curvature.

V. SUMMARY AND CONCLUSIONS

We have investigated the phase behavior and scattering intensities of ternary microemulsions of water, oil and nonionic surfactant, containing in addition small amounts of amphiphilic diblock copolymers. The effect of the block copolymer on the phase behavior is to drastically enhance the efficiency of the surfactant, i.e., the same amount of oil and water can be solubilized with a much smaller total amount of amphiphile. This effect has first been reported in Ref. 1.

The careful analysis of the partial structure factors, which were obtained from neutron scattering data by a sophisticated contrast variation scheme, provides very detailed information on the structure of the microemulsion phase on mesoscopic scales, and the conformation of the polymers and their location relative to the surfactant film. This is an essential requirement for a comparison with theoretical approaches—and for a detailed understanding of the mechanism by which amphiphilic block copolymers affect the properties of membrane ensembles. We find that in the mushroom regime, our scattering data are consistent with polymer coils, which behave as self-avoiding chains anchored to an (almost) planar surface. The mushrooms are distributed uniformly on the membrane. The presence of any block copolymer aggregates (micelles) can be excluded.

As the scattering results show, block copolymers in ternary microemulsions have the further advantage that they allow for a controlled and systematic variation of the density of polymers anchored to the interface membrane. Thereby, following the theoretical expectation,[39] bending rigidity and the saddle-splay modulus may be controlled, which in the mushroom regime are simply linear functions of the polymer concentration on the membrane. A similar variation occurs, of course, in mixtures of two surfactants,[68] but the dependence in general is more complicated due to the badly understood molecular origin of the curvature moduli in this case. Therefore, the ternary system with additional block copolymer is very well suited for a stringent test of current theories of amphiphilic systems. We have compared, in particular, the film scattering data with the theoretical results of both a Ginzburg–Landau theory and a Gaussian-random-field model. In the latter approach, we propose an approximate analytical expression for the scattering intensity, based on the results of Ref. 22 for the film correlation function, which reproduces the known exact results for the Q dependence at small and large wave vectors Q. In both cases, the theoretical expressions fit the data very well. In the Ginzburg–Landau approach, the fitting parameters are the coupling constants, which describe the interaction of the local amphiphile density with the concentration difference of oil and water. In the Gaussian-random-field model, the fitting parameters are related to the average amphiphile concentration and the bending rigidity of the membrane. Therefore, for the present system of a sharp and saturated interface film, the latter approach seems more appropriate.

Our scattering results imply that the block copolymers are uniformly distributed on the membrane. We therefore propose that the phase behavior can be understood from the effect of the anchored polymer on the curvature moduli of the membrane. Indeed, we find that this hypothesis leads to a prediction for the scaling form of the emulsification phase boundary, which is fully consistent with the experimental observations. The amplitude in this scaling form is about a factor of 2 larger than the theoretical result for *ideal chains*. We believe that this difference arises from the different scaling behaviors of polymers in good and in theta solvents.

Our experiment provides the first investigation that by application of a consistent model, allows to infer the behavior of the (effective) saddle-splay modulus as a function of the anchoring density. Therefore, no comparison with other experiments on this quantity is possible. However, there are

Reuse of AIP Publishing content is subject to the terms: https://publishing.aip.org/authors/rights-and-permissions. Downloaded to IP: 145.94.180.253 On: Thu, 17 Mar 2016 15:06:52

several measurements of the (effective) bending rigidity. Of these, the experiment of Evans and Rawicz[10] provides the most quantitative results, and also is the only one where the molecular-weight dependence of the polymer is investigated. They observe a leveling off of the bending rigidity for large (total) polymer concentrations,[9,10] which is obviously due to the fact that the polymer is no longer anchored to the membrane, but forms micelles or other aggregates in solution. The amplitude of the scaling law was found to be about a factor 4 to 5 larger in Ref. 10 than predicted for ideal chains, which is about a factor 2 more than what we see for $\overline{\kappa}$. However, it is more disturbing to see that the linear dependence of κ_{eff} on the grafting density extends about a factor of 10 beyond the overlap concentration. It it not at all obvious, of course, that the *definition* $\sigma R_e^2=1$ of the overlap concentration with the end-to-end distance R_e is the best choice to describe the crossover from the mushroom to the brush regime, or whether $\sigma R_g^2=1$ with the radius-of-gyration $R_g=R_e/\sqrt{6}$ might not be more appropriate. We can employ the results for the crossover from the dilute to the semidilute regime in bulk polymer solutions to provide some guidance. In this case, the crossover is observed experimentally in terms of the concentration dependence of the osmotic pressure[69] somewhat below the point $\sigma R_g^3=1$. Thus, it is conceivable that most of the data in Ref. 10 are taken effectively in the mushroom regime. It is also possible that other effects, like an adsorption of the PEO chain to the lipid membrane, are responsible for enhancement of the polymer effect on the membrane rigidity as observed in Ref. 10. In any case, it will be interesting to see what happens in our system at higher grafting densities.

Applying the concepts and methods presented in our paper renders the bicontinuous microemulsion phases into a tool to investigate the membrane modification properties of (polymeric) cosurfactants. It is, however, necessary that the system stays in the bicontinuous phase and mediated interaction of adjacent membranes are negligible. Observing these caveats, there are several other interesting possibilities to investigate, how hydrophobic, hydrophilic or amphiphilic polymers modify the curvature elasticity in these systems. An obvious candidate are nonadsorbing hydrophilic homopolymers. The effect of such polymers in binary water-surfactant systems has been studied in Refs. 70 and 71. The effect on the phase behavior, however, will certainly be smaller in mixtures containing hydrophilic or hydrophobic homopolymers, since the polymer is distributed almost uniformly in the oil and/or water regions, while only the polymers close to the surfactant membrane will affect its curvature properties.

APPENDIX A: SYNTHESIS OF BLOCK COPOLYMERS

The PEP–PEO block copolymers were synthesized by anionic polymerization. All manipulations were performed under high vacuum in glass reactors provided with break seals for the addition of reagents. The preparation of the initiators and the purification procedures for monomers and solvents to the standard required for anionic polymerization have been described elsewhere.[27,28]

The anionic polymerization of the block copolymer was realized in a two-step process, because the synthesis of the two blocks requires different reaction conditions. In the first step isoprene was polymerized in benzene with size exclusion chromatography butyllithium as initiator. The endcapping with ethylene oxide (EO) yielded polyisoprene functionalized with a hydroxyl endgroup PI–OH. The polymer was hydrogenated with H_2 to the corresponding PEP–OH using a conventional Pd/BaSO4 catalyst. In the second polymerization step, cumylpotassium was used to transfer PEP–OH into the macroinitiator PEP–OK. The PEP–PEO block copolymers were obtained after polymerizing the calculated amounts of EO in THF at 50 °C for 3 days. The reaction was terminated with acetic acid and the product was precipitated twice in acetone at −10 °C to −20 °C.

The number average molecular weight M_n of the PEP–OH was obtained from the titration with the highly colored cumylpotassium. Knowing the amount of PEP–OH and the concentration of the cumylpotassium solution, the titration can be considered as endgroup analysis for the determination of M_n. The deuterium contents of the partially deuterated PEP–OH samples were measured by ^{1}H–NMR spectroscopy using a 500 MHz Bruker spectrometer. Known amounts of the polymer and $C_2H_2Br_4$ as reference were dissolved in $CDCl_3$. The comparison of the $C_2H_2Br_4$ signal intensity at 6.1 ppm with the signal intensities of the PEP protons between 1 and 2 ppm allowed to calculate the deuterium contents. The block copolymer compositions were also calculated by ^{1}H–NMR spectroscopy, comparing the PEP signals with the PEO signal at 3.6 ppm and taking into account the deuterium content of the PEP–OH. From the compositions and the titration molecular weights of the PEP–OH the block copolymer molecular weights were obtained. Molecular weight distributions were obtained by size exclusion chromatography (SEC) using a Waters 150C instrument at 30 °C. THF was the eluent for the PEP–OH and a mixture of 90 vol % THF and 10 vol % DMA was used for the block copolymers.

In order to perform experiments under polymer contrast, a fully deuterated $C_{10}E_4$ had to be synthesized. Several synthetic strategies were checked with respect to product yield and costs of the different deuterated components. Finally, the oligomerization of deuterated potassium *n*-decanolate with deuterated ethylene oxide was chosen as the most economic process. The potassium *n*-decanolate was obtained by reacting potassium metal with a small excess of *n*-decanol-d_{22} (CDN isotopes) under argon atmosphere. No solvent was used in this step because of solubility difficulties of the product in common aprotic, polar solvents at room temperature and reaction of potassium metal with those solvents at elevated temperature. After 5 days at 70 °C almost all potassium metal disappeared. The potassium *n*-decanolate was then dissolved in 1,3 dimethyltetrahydro-2-(1H)-pyrimidinone (DMPU) (Merck) at 100 °C. The required amount of ethylene oxide-d_4 (EO) (CDN isotopes) corresponding to the stoichiometry of d-$C_{10}E_4$ was added via the gas phase. The EO as well as the DMPU were dried before use by stirring over calcium hydride overnight followed by distillation under reduced pressure. The reaction mixture was

Reuse of AIP Publishing content is subject to the terms: https://publishing.aip.org/authors/rights-and-permissions. Downloaded to IP: 145.94.180.253 On: Thu, 17 Mar 2016 15:06:52

left for 1 h at 100 °C and overnight at room temperature. Then the required amount of HCl was added, the product dissolved in diethyl ether, and washed with water in order to remove DMPU and KCl. The diethyl ether was evaporated under reduced pressure and the raw product stirred under high vacuum for 1 h to remove residues of diethyl ether and water.

The product composition was evaluated by SEC using THF as solvent and a refractive index detector. The use of two ultrastyragel columns of 500 and 1000 Å pore size yielded sufficient separation efficiency to analyze the surfactant mixture. It was found that the product contained 20% of d-$C_{10}E_4$. Due to the relatively large amount of approximately 33 g, the raw product was prepurified by distillation. A 20 cm Vigreux column was used and high vacuum was necessary. A fraction of 8 g was obtained that contained 75% of d-$C_{10}E_4$ together with 19% of d-$C_{10}E_3$ and 6% of d-$C_{10}E_5$ as analyzed by SEC. This mixture was purified in a second step by chromatography on a silica gel column eluted with ethyl acetate. 5.2 g of the product were obtained after evaporation of the solvent and removal of volatile residues under high vacuum. SEC was found not to be sensitive enough to detect small amounts of byproducts. For that reason thin layer chromatography (TLC) was used to evaluate the product purity. This technique allowed to detect relative amounts of much less than 1% of d-$C_{10}E_3$ or d-$C_{10}E_5$ in the product as found by analyzing surfactant mixtures of known composition. The TLC investigation showed that the product contained pure d-$C_{10}E_4$, no byproduct was found.

The deuterium content of $C_{10}E_4$ was checked by ^{1}H–NMR. Known amounts of d-$C_{10}E_4$ and $C_2H_2Br_4$ as reference were dissolved in $CDCl_3$. The comparison of the $C_2H_2Br_4$ signal intensity at 6.1 ppm with the signal intensities of the E_4 unit at 3.6 ppm and the C_{10} unit between 0.8 and 1.5 ppm and at 3.4 ppm allowed to calculate the deuterium contents. For the E_4 unit, except the OH endgroup, 99.8 atom % deuterium and for the C_{10} unit 98.9 atom % deuterium were found.

In order to determine the phase behavior, samples were prepared with hydrogenous compounds. Water was deionized and twice distilled, *n*-decane was obtained from SIGMA (Steiner, Germany) with a purity >99% and $C_{10}E_4$ was purchased from Bachem (Bubendorf, Switzerland) with purity >98%. All substances were used without further purification.

APPENDIX B: FILM SCATTERING FUNCTIONS

The rather lengthy expression for the function $I_1 \cdots I_3$ in the expression for the film scattering in Sec. III B 3 are given by

$$I_1(x,y) = \Lambda_-(x,y), \tag{B1}$$

$$I_2(x,y) = -\left(1+\frac{1}{2}x^2-y^2\right)\Lambda_-(x,y)+y \quad \Xi_0(x,y), \tag{B2}$$

$$\begin{aligned} I_3(x,y) = {} & \tfrac{1}{6}(-6-39x^2+42y^2+x^4+6y^4)\Lambda_-(x,y) \\ & + \tfrac{2}{3}x(-8+3x^2-3y^2)\Omega(x,y) \\ & - \tfrac{2}{3}xy(3+y^2)\Lambda_0(x,y)+y(5+y^2) \\ & \Xi_0(x,y)+\tfrac{4}{3}y^2. \end{aligned} \tag{B3}$$

Here, we have defined a number of elementary functions:

$$\Lambda_\pm(x,y) = \frac{1}{4x}\left[2\arctan\left(\frac{x}{2}\right) \pm \arctan\left(\frac{4x}{4+4y^2-x^2}\right) \pm n\pi\right], \tag{B4}$$

where $n=1$ for $x^2>(4+4y^2)$ and $n=0$ otherwise,

$$\Lambda_0(x,y) = \frac{1}{2x}\left[\arctan\left(\frac{x+2y}{2}\right) - \arctan\left(\frac{x-2y}{2}\right)\right], \tag{B5}$$

$$\Omega(x,y) = \frac{1}{8x}\left[\ln\left(\frac{4+(2y-x)^2}{4+x^2}\right) + \ln\left(\frac{4+(2y+x)^2}{4+x^2}\right)\right], \tag{B6}$$

$$\Xi_0(x,y) = \frac{1}{4x}\ln\left(\frac{4+(2y+x)^2}{4+(2y-x)^2}\right). \tag{B7}$$

With these definitions, the vertex function $\Gamma(x,y)$ in Eq. (34), which has been calculated in Ref. 58, is given by

$$\begin{aligned} \frac{\xi^2}{2\alpha}\Gamma(x,y) = {} & (\gamma_1-\gamma_2 x^2)^2\,\Lambda_-(x,y)+2\gamma_3(\gamma_1-\gamma_2 x^2) \\ & \times[(1-y^2)\Lambda_-(x,y)-y\Xi_0(x,y)] \\ & + \gamma_3^2\{2y^2[\Lambda_+(x,y)-\Lambda_-(x,y)] \\ & + (1-y^2)^2\Lambda_-(x,y)-2y(1-y^2) \\ & \times\Xi_0(x,y)+y^2\}, \end{aligned} \tag{B8}$$

where $\gamma_1=\tilde{\gamma}_1 A\xi\sqrt{(4\pi\xi)/\alpha}$, $\gamma_2=\tilde{\gamma}_2 A\xi^{-2}\xi\sqrt{(4\pi\xi)/\alpha}$, and $\gamma_3=\tilde{\gamma}_3 A\xi^{-2}\xi\sqrt{(4\pi\xi)/\alpha}$; the amplitude A is defined in Eq. (33).

[1] B. Jakobs *et al.*, Langmuir **15**, 6707 (1999).
[2] T. M. Allen and A. Chonn, FEBS Lett. **223**, 42 (1987).
[3] A. Gabizon and D. Papahadjopoulos, Proc. Natl. Acad. Sci. U.S.A. **85**, 6949 (1988).
[4] D. D. Lasic, *Liposomes: From Physics to Applications* (Elsevier, New York, 1993).
[5] D. D. Lasic and D. Papahadjopoulos, Science **267**, 1275 (1995).
[6] *Stealth Liposomes*, edited by D. D. Lasic and F. J. Martin (CRC, Boca Raton, FL, 1995).
[7] H. E. Warriner *et al.*, Science **271**, 969 (1996).
[8] H. E. Warriner *et al.*, Biophys. J. **75**, 272 (1998).
[9] Y. Yang *et al.*, Phys. Rev. Lett. **80**, 2729 (1998).
[10] E. A. Evans and W. Rawicz, Phys. Rev. Lett. **79**, 2379 (1997).
[11] R. Joannic, L. Auvray, and D. D. Lasic, Phys. Rev. Lett. **78**, 3402 (1997).
[12] M. Teubner and R. Strey, J. Chem. Phys. **87**, 3195 (1987).
[13] K.-V. Schubert, R. Strey, S. R. Kline, and E. W. Kaler, J. Chem. Phys. **101**, 5343 (1994).
[14] R. Strey, Curr. Opin. Colloid Interface Sci. **1**, 402 (1996).
[15] M. Gradzielski, D. Langevin, T. Sottmann, and R. Strey, J. Chem. Phys. **104**, 3782 (1996).
[16] T. Sottmann, R. Strey, and S.-H. Chen, J. Chem. Phys. **106**, 6483 (1997).
[17] G. Gompper and M. Schick, in *Phase Transitions and Critical Phenomena*, edited by C. Domb and J. Lebowitz (Academic, London, 1994), Vol. 16, pp. 1–176.

Reuse of AIP Publishing content is subject to the terms: https://publishing.aip.org/authors/rights-and-permissions. Downloaded to IP: 145.94.180.253 On: Thu, 17 Mar 2016 15:06:52

[18] D. Roux *et al.*, Europhys. Lett. **11**, 229 (1990).
[19] D. Roux, C. Coulon, and M. E. Cates, J. Phys. Chem. **96**, 4174 (1992).
[20] G. Gompper and M. Schick, Phys. Rev. E **49**, 1478 (1994).
[21] P. Pieruschka and S. A. Safran, Europhys. Lett. **22**, 625 (1993).
[22] P. Pieruschka and S. A. Safran, Europhys. Lett. **31**, 207 (1995).
[23] D. C. Morse, Phys. Rev. E **50**, R2423 (1994).
[24] L. Golubović, Phys. Rev. E **50**, R2419 (1994).
[25] G. Gompper and D. M. Kroll, Phys. Rev. Lett. **81**, 2284 (1998).
[26] H. Endo *et al.*, Phys. Rev. Lett. **85**, 102 (2000).
[27] J. Allgaier, A. Poppe, L. Willner, and D. Richter, Macromolecules **30**, 1582 (1997).
[28] A. Poppe *et al.*, Macromolecules **30**, 7462 (1997).
[29] J. W. Mays and L. J. Fetters, Macromolecules **22**, 921 (1989).
[30] L. J. Fetters (unpublished).
[31] S. Burauer, T. Sachert, T. Sottmann, and R. Strey, Phys. Chem. Chem. Phys. **1**, 4299 (1999).
[32] G. E. Bacon, *Neutron Diffraction* (Claredon, Oxford, 1975), p. 561.
[33] G. Gompper and M. Schick, Phys. Rev. Lett. **62**, 1647 (1989).
[34] G. Porod, in *Small Angle X-ray Scattering*, edited by O. Glatter and O. Kratky (Academic, New York, 1982).
[35] D. Richter *et al.*, Macromolecules **30**, 1053 (1997).
[36] R. Strey, J. Winkler, and L. Magid, J. Phys. Chem. **95**, 7502 (1991).
[37] P. B. Canham, J. Theor. Biol. **26**, 61 (1970).
[38] W. Helfrich, Z. Naturforsch. C **28c**, 693 (1973).
[39] C. Hiergeist and R. Lipowsky, J. Phys. II **6**, 1465 (1996).
[40] E. Eisenriegler, A. Hanke, and S. Dietrich, Phys. Rev. E **54**, 1134 (1996).
[41] C. M. Marques and J. Fournier, Europhys. Lett. **35**, 361 (1996).
[42] S. T. Milner and T. A. Witten, J. Phys. (France) **49**, 1951 (1988).
[43] S. Leibler and D. Andelman, J. Phys. (France) **48**, 2013 (1987).
[44] M. M. Kozlov and W. Helfrich, Langmuir **8**, 2792 (1992).
[45] R. Lipowsky, Europhys. Lett. **30**, 197 (1995).
[46] F. Castro-Roman, G. Porte, and C. Ligoure, Phys. Rev. Lett. **82**, 109 (1999).
[47] S. A. Safran, D. Roux, M. E. Cates, and D. Andelman, Phys. Rev. Lett. **57**, 491 (1986).
[48] D. Andelman, M. E. Cates, D. Roux, and S. A. Safran, J. Chem. Phys. **87**, 7229 (1987).
[49] L. Golubović and T. C. Lubensky, Phys. Rev. A **41**, 4343 (1990).
[50] F. David, in *Statistical Mechanics of Membranes and Surfaces*, edited by D. Nelson, T. Piran, and S. Weinberg (World Scientific, Singapore, 1989), pp. 157–223.
[51] R. Hołyst and M. Schick, J. Chem. Phys. **96**, 7728 (1992).
[52] N. F. Berk, Phys. Rev. Lett. **58**, 2718 (1987).
[53] N. F. Berk, Phys. Rev. A **44**, 5069 (1991).
[54] M. Teubner, Europhys. Lett. **14**, 403 (1991).
[55] P. Pieruschka and S. Marčelja, J. Phys. II **2**, 235 (1992).
[56] M. Teubner, J. Chem. Phys. **92**, 4501 (1990).
[57] E. Eisenriegler, K. Kremer, and K. Binder, J. Chem. Phys. **77**, 6296 (1982).
[58] G. Gompper and M. Schick, Phys. Rev. B **41**, 9148 (1990).
[59] T. Sottmann and R. Strey, J. Chem. Phys. **106**, 8606 (1997).
[60] T. Hellweg and D. Langevin, Phys. Rev. E **57**, 6825 (1998).
[61] L. Peliti and S. Leibler, Phys. Rev. Lett. **54**, 1690 (1985).
[62] W. Cai, T. C. Lubensky, P. Nelson, and T. Powers, J. Phys. II **4**, 931 (1994).
[63] P. Auroy, L. Auvray, and L. Leger, J. Phys.: Condens. Matter **2**, 317 (1990).
[64] P. Auroy and L. Auvray, J. Phys. II **3**, 227 (1993).
[65] L. Auvray and P.-G. de Gennes, Europhys. Lett. **2**, 647 (1986).
[66] S. Kawaguchi *et al.*, Polymer **38**, 2885 (1997).
[67] G. Beaucage, J. Appl. Phys. **29**, 134 (1996).
[68] M. Gradzielski, D. Langevin, T. Sottmann, and R. Strey, J. Chem. Phys. **106**, 8232 (1997).
[69] I. Noda, N. Kato, T. Kitano, and M. Ngasawa, Macromolecules **8**, 668 (1981)
[70] C. Ligoure, G. Bouglet, and G. Porte, Phys. Rev. Lett. **71**, 3600 (1993).
[71] G. Bouglet *et al.*, Phys. Rev. E **57**, 834 (1998).

Reuse of AIP Publishing content is subject to the terms: https://publishing.aip.org/authors/rights-and-permissions. Downloaded to IP: 145.94.180.253 On: Thu, 17 Mar 2016 15:06:52